RSC Advances

REVIEW

View Article Online
View Journal | View Issue

Cite this: *RSC Adv.*, 2025, **15**, 28093

MXene based nanoarchitectures for organic contaminants degradation under sonophotocatalytic environment: eco-friendly synthesis, catalytic attributes and recent advancements

S. K. Sheik Moideen Thaha and Panneerselvam Sathishkumar *

The 6th and 12th Sustainable Development Goals (SDGs) focus on reducing environmental pollution and improving sanitation through responsible production and consumption. However, current wastewater treatment technologies fall short, with projections indicating that up to 4.8 billion people may face health issues due to inadequate water purification by 2030. Preventing environmental problems is more effective than addressing their consequences. Hybrid advanced oxidation processes (h-AOPs), such as sonophotocatalysis, offer a sustainable and efficient method for catalytic conversion, decomposing environmental toxins in water without secondary pollution. Recently, MXene-based nanocatalysts have attracted attention due to their unique properties, including high surface area, excellent adsorption capabilities, and internal electric fields, making them ideal for AOP-related applications. This review comprehensively discusses the synergistic benefits of sonophotocatalysis for the degradation of various organic pollutants, sustainable synthesis routes for MXene and its precursor (MAX) and their alignment with SDG targets. We have reviewed various reports on MXene-based nanocatalysts for contaminant mineralization, systematically tabulated recent advancements. The optical properties and heterojunction-driven charge carrier migration were discussed with respect to novel MXene-based nanocomposites. Finally, future perspectives on MXene-based nanoarchitectures, synergistic ultrasonic approaches and greener approaches to minimize secondary pollution are outlined to support effective AOP-assisted wastewater treatment.

Received 10th June 2025
Accepted 28th July 2025

DOI: 10.1039/d5ra04096e

rsc.li/rsc-advances

Ultrasonics and Advanced Photochemistry Lab, Department of Chemistry, School of Advanced Sciences, Vellore Institute of Technology, Vellore 632014, India. E-mail: sathishkumar.p@vit.ac.in

S. K. Sheik Moideen Thaha

Sheik Moideen Thaha S. K. is a doctoral research scholar at Vellore Institute of Technology (VIT) Vellore, India. His area of research interest includes 2D materials, surface-engineered nanomaterials, ultrasonics, and reactor systems. He is currently working in the Ultrasonics and Advanced Photochemistry Laboratory under the supervision of Dr Sathishkumar P., focusing on the development of custom-designed synergy reactors integrating ultrasound and visible light for the degradation of environmental toxins. His research emphasizes the synthesis and application of novel nanocomposites for advanced oxidation processes, aiming to advance efficient and sustainable methods for water purification and environmental remediation.

Panneerselvam Sathishkumar

Sathishkumar Panneerselvam began his research in nanomaterials and photocatalysis in the year 2007 and he earned his PhD from the National Institute of Technology (NIT), Tiruchirappalli, India in 2010 and later pursued post-doctoral research at the University of Concepción, Chile. With over 15 years of experience in sonochemistry, photocatalysis and nanomaterials, he has published more than 60 original research articles, ten book chapters and edited two books in Springer nature and IOP publications. He has held various research positions in the international level. After joining Vellore Institute of Technology (VIT), Vellore, India as an Assistant Professor, he has led the Ultrasonics and Advanced Photochemistry Laboratory since 2020.

1. Introduction

Alarming projections reveal that unless urgent action is taken, 4.8 billion people will be exposed to hazardous health risks and economic instability by 2030, stemming from the world's current wastewater treatment and water quality shortcomings.[1] The urgency of this forecast has sparked a rise in research focused on sustainable, eco-friendly strategies for eliminating aquatic toxins. As the global community strives to achieve the (Sustainable Development Goals) SDGs, particularly in wastewater treatment, there is a heightened focus on promoting eco-innovations that prioritize scalability, sustainability, and pollution prevention. Conventional wastewater treatment technologies, including ozone treatment, direct-radical promoter treatment and other oxidant-based methods, often generate secondary pollution through oxidant leaching.[2–4] These homogeneous catalytic treatments pose significant challenges in achieving the Sustainable Development Goals (SDGs) while also meeting cost-effectiveness requirements.[5] With the world's population projected to reach 8.2 billion and beyond, there is an urgent need for a robust system that can neutralize deadly toxins without causing secondary pollutionIn response, researchers have increasingly turned to hybrid advanced oxidation processes (h-AOPs) and novel nanocatalysts like MXene, which boasts outstanding catalytic capabilities.[6]

The success of h-AOP technology is primarily attributed to the synergistic effects, which enhance efficiency, reduce treatment time, and improve cost-effectiveness.[7] The reactive oxygen species (ROS) are generated *in situ* during treatment and are highly reactive in oxidizing the toxic organic and inorganic residues present in the aquatic ecosystem. There are various individual AOP technologies, each producing ROS through distinct processes. In brief, photocatalytic processes generate free radicals by separating electron–hole pairs at the semiconductor, which causes a redox reaction and the production of reactive species. On the other hand, physical processes like sonocatalysis generates free radicals through the acoustic cavitation which involves the collapse of unstable bubbles. Alternatively, chemical processes like Fenton or Fenton-like processes primarily produce free radicals through the exchange of variable redox potentials of metals and H_2O_2. The ozone process is characterised by the production of reactive free radicals by the electrophilic O_3. The h-AOPs is achieved by combining two or more treatment methods. When analyzing the potential h-AOPs opportunities in light of the SDGs and cost-effectiveness, the ultrasound-assisted photocatalysis (sonophotocatalysis) is considered to be the most promising technology.[8] The combined irradiation of the ultrasound and light energy offers the prospect of sustainability and an eco-friendly nature. Moreover, the irradiation of ultrasound (US) and light energy enables scalable opportunities for industrial-level wastewater treatment, with reduced time and economic aspects. These remediation strategies are particularly vital due to the increased presence of persistent organic pollutants (POPs) such as antibiotics, dyes, pesticides and pharmaceutical residues in wastewater.[9] These POPs often originate from domestic discharge, textile industries, and agricultural runoff, and are known for their lethal toxicity, bioaccumulation and long-term ecological harm.[10] Their resistance to conventional treatment poses a serious risk to aquatic ecosystem. Therefore, understanding the degradation mechanisms of such pollutants under hybrid AOPs, especially sonophotocatalysis, is essential for designing targeted and efficient detoxification systems.

The mechanism of US-assisted photocatalysis involves the acoustic cavitation of bubbles and photoinduced excitation of electrons within the semiconductor nanocatalyst. Notably, materials with superior surface features tend to exhibit significant enhancements in the US-assisted catalytic process (sonocatalysis). Furthermore, nanomaterials with broad light absorption and distinct semiconductor properties demonstrate superior photocatalytic activity due to their efficient light-harvesting capabilities and ROS generation potential such as TiO_2, ZnO, r-GO and g-C_3N_4.[11,12] However, in the context of US-assisted sonophotocatalysis, the properties of the nanocatalyst are more critical than those of individual AOPs as the nanocatalyst must actively participate in the generation of ROS while also facilitating synergistic interactions to effectively decompose toxic substances in water environments. In this regard, various nanocatalysts supported by carbon-based materials such as carbon nanotubes, graphitic nanodiamonds, and carbon nanorods have recently been employed to enhance catalytic efficiency.[13] However, these materials face significant challenges including low mass transfer, leaching from the aqueous medium, photocorrosion, and difficulties in selective synthesis.[14] The leaching of supported metal ions presents an additional challenge contributing to secondary pollution during the oxidation process and complicating their removal.[15] Although some traditional nanocatalysts such as TiO_2 and ZnO have demonstrated improved US-assisted photocatalytic efficiency against various environmental contaminants in recent years, they have exhibited persistent issues such as photocorrosion, low surface area, poor responsiveness to direct solar light, and rapid charge recombination.[16–19] These challenges require focused attention to advance research and develop superior nanocatalysts suitable for industrial-scale applications more preferably h-AOP.

In the 21st century, often regarded as the era of nanoscience and nanotechnology, metal carbides and nitrides have attracted significant interest from a wide range of research communities.[20] The primary foundation of this attraction lies in their potential for wide combinations and tunability to suit specific applications.[21] Numerous nanostructures have been developed and studied to enhance their characteristic features, such as surface area and surface terminal properties.[22,23] Among these, the 1st breakthrough occurred in 2011 when Naguib *et al.* discovered 2D layered metal carbides by etching the MAX phase of titanium-based ceramic to derive 2D MXenes ($Ti_3C_2T_x$).[24] Since then, there has been an exponential increase in research interest in MXenes in various dimensions of research, as illustrated in Fig. 1a. The distinctive properties observed in MXenes, such as high surface area, excellent conductivity, layered structure, unique electronic features, heterogeneity, and remarkable mechanical qualities, are the paramount rationale

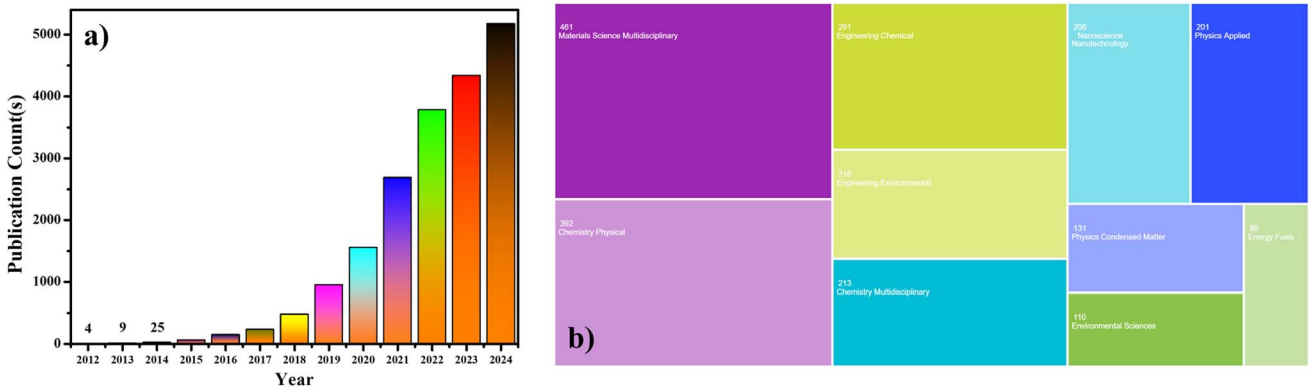

Fig. 1 (a) Statistics on number of research publications related to MXene since its discovery (2011) (b) web of science publications categories available on MXene for selected keywords {keywords; (a) MXene (b) MXene and photocatalysis}. Obtained from the Web of science.

behind the exponential growth in research interest. WOS category analysis demonstrated significant attention towards multidisciplinary and fundamental research with a dominant focus on environmental and energy-related applications (Fig. 1b). MXenes are synthesized by etching the "A" layer from 3D MAX phases to produce 2D layered MX phases. Consequently, chemical routes are preferentially utilized to remove the A layer and prepare MXenes. The interlayer distance plays a critical role in tuning the resulting MXenes into various forms, including lamellar nanosheets, accordion-like multilayers, stacked layers, and monolayers. As a result, MXenes hold significant potential for applications in h-AOPs as well as in single-handed AOPs, owing to their exceptional attributes.

The novelty of the current study lies in consolidating a comprehensive understanding of the ultrasound (US) mechanism, the synergistic effects derived from the sonophotocatalytic process, and perspectives on greener approaches for synthesizing MAX phases and MXenes, along with their concurrent applications in degrading various hazardous water contaminants. Currently, no literature provides such an in-depth and comprehensive analysis of the US mechanism and its synergism along in the context of SDG-oriented synthesis of MAX and MX phases. However, few review articles/chapters have focused on MXenes as emerging sonocatalysts for the removal of pharmaceutical pollutants.[25,26] The motivation behind this study is to present a complete review that demonstrates how US-based processes, particularly sonophotocatalysis, can effectively activate MXene-based nanoarchitectures and to explore their future prospects through greener synthetic strategies. The primary databases used to collect relevant literature include Web of Science, Scopus, and SciFinder. The selected papers were arranged and tabulated chronologically under three categories: sonophotocatalysis, sonocatalysis, and photocatalysis. A targeted search was conducted for MXene-based nanocatalysts in environmental remediation using keywords such as MXene, photocatalysis, sonocatalysis, dyes, antibiotics, pesticides, and effluents (2015 to 2025). Each collected study was interpreted based on the process type, pollutant, and the mechanism followed by the nanocatalyst. Papers were then selected for discussion based on their relevance to the study objectives. Notably, many MXene based nanocatalysts were reported with Z-scheme and S-scheme mechanisms, therefore, some results were excluded if already covered in existing reviews. Instead, few novel and interesting nanostructures were discussed to maintain the comprehensiveness of this review. The greener synthesis approaches for MAX and MX phases were compiled through manual searches using broader terms. These findings were interpreted and summarized to align with the study's focus on methods for MAX and MX synthesis, use of greener chemicals, alternative etching approaches, etching time, and their respective outcomes.

In recent high-impact studies of MXenes and MXene-based nanocatalysts have attracted significant attention for environmental applications, particularly in the removal of organic and inorganic pollutants. Consequently, only a few reviews have explored the catalytic efficiency of MXenes for environmental remediation. However, these reviews have largely overlooked the potential of sonocatalysis and hybrid advanced oxidation processes (h-AOPs), particularly in the context of US-assisted photocatalysis.[27,28] Notably, research on h-AOPs, specifically sonophotocatalysis, remains in its infancy. As a consequence, updates on the latest advancements related to MXene-based nanocatalysts for sonophotocatalysis are indispensable. These updates reflects the foundational understanding of the role of US and the underlying mechanisms driving these synergism. Therefore, the motivation of our current study is to provide comprehensive insights into sonocatalytic processes, the synergism of h-AOPs (US and light energy), SDGs intented synthesis routes for MAX and MXene phases, MXene-based heterojunction engineering for organic contaminants removal, synergistic effects and future perspectives.

2. Role of ultrasound in environmental cleaning

The importance of soundwaves in science and engineering has grown substantially as a result of multitude use cases. As a result, sonochemistry plays a vital part in the disintegration of pollutant, from the pretreatment of sludges from industrial waste to tertiary treatment.[29,30] Sonocatalysis differs from

conventional oxidation processes such as Fenton or ozonation by generating enormous quantities of energy in the aquatic environment without developing any secondary pollution.[31] Sonocatalysis is considered relatively more sustainable than conventional oxidation processes and could serve as a promising green alternative, particularly if the required ultrasound energy is generated through renewable sources such as solar cells, fuel cells, or other renewable energies. In contrast, visible-light-driven photocatalysis may be constrained by seasonal variations and geographic location.[32,33] Consequently, it makes sonocatalysis a superlative technology among other oxidation process.

Sonochemical effects are the result of sound energy traveling through an aqueous media. The process known as cavitation is one of the sonochemical effects and produces the extreme energy required to destroy or disrupt the contaminant. In general, soundwaves are classified based on its frequency range as shown in Fig. 2a. A sonochemical effect causes unique cavitation events (acoustic, hydrodynamic, optic and particle cavitation) depending on the frequency range, method of generation, and sound parameters (power, intensity, solvent, shape of reactor).[34,35] In contrast to optic and particle cavitations, hydrodynamic and acoustic cavitations are more ideally suited to oxidize contaminants present within the medium. Acoustic cavitations produces more violent energy since it is induced by pressure flocculation in the passageway of sound. The accumulation of energy in a narrow area creates massive physiochemical conditions. Sonocatalysis has been explained by a few mechanisms, including heterogeneous nucleation, photocatalytic excitation, and thermal excitation.

2.1 Mechanism of cavitational bubble generation and sonocatalysis

Sound is made up of pressure waves in the form of longitudinal that are transmitted as a cycle of compression and rarefaction. In a sonochemical or sonocatalytic method, the ultrasonic waves are passed through the solution in the range of 20–1000 kHz using an ultrasonicator.[36] The transmitted sound waves give rise to the formation of cavity bubbles. These bubbles are extremely small, confined, and serve as micro-reactors in the aqueous system. The ultrasonic waves outstrips the attractive forces in the water molecules, which leads to a event referred as cavitation event that include the nucleation, formation, growth, and collapse of the bubbles. The implosive collapse of bubbles generates an extremely localised temperature of about 5000 K, pressure of about 500 atm and exhibit radiation in the range of 200–800 nm which is known as sonoluminescence (SL).[37] The cavitational events are divided into two category; stable and transient. Stable events result in less implosive collapse than transient cavitation, thus making transient cavitation more effective for sonocatalysis. The mechanism of acoustic cavitation is shown Fig. 2b.

2.1.1 Mechanisms of sonocatalysis. To understand the phenomenon of sonocatalysis, we need to understand the region and surroundings of bubble cavity (hotspot). The region of bubble cavity is shown in Fig. 2c.

(i) The region inside the bubble cavity also known as supreme reactor region. Here most of the pyrolytic reactions (water splitting) as well as hydroxyl radical reactions occurs at small extent. This region is known as pyrolytic reactions zone and the process is known as sonolysis. Superior physical conditions are observed in this region (*i.e.*) 5000 K, 500 atm and sonoluminescence.

(ii) The region at bubble-liquid layer or interface is known as hydroxyl radical reactions zone since predominant reactions are occurs through $OH^{\bullet}$ radical pathway. Here the physical conditions are lighter than in (i) but the formation and reaction flow of $OH^{\bullet}$ radicals and H_2O_2 was predominant.

(iii) The region outside (i) and (ii) is bulk liquid which is also known as secondary sonochemical reaction zone. The radicals that jump from the (i) and (ii) undergoes secondary reactions here. Hydrogen, hydroxyl, peroxyl radicals, molecular oxygen and hydrogen peroxide are generated in this region.

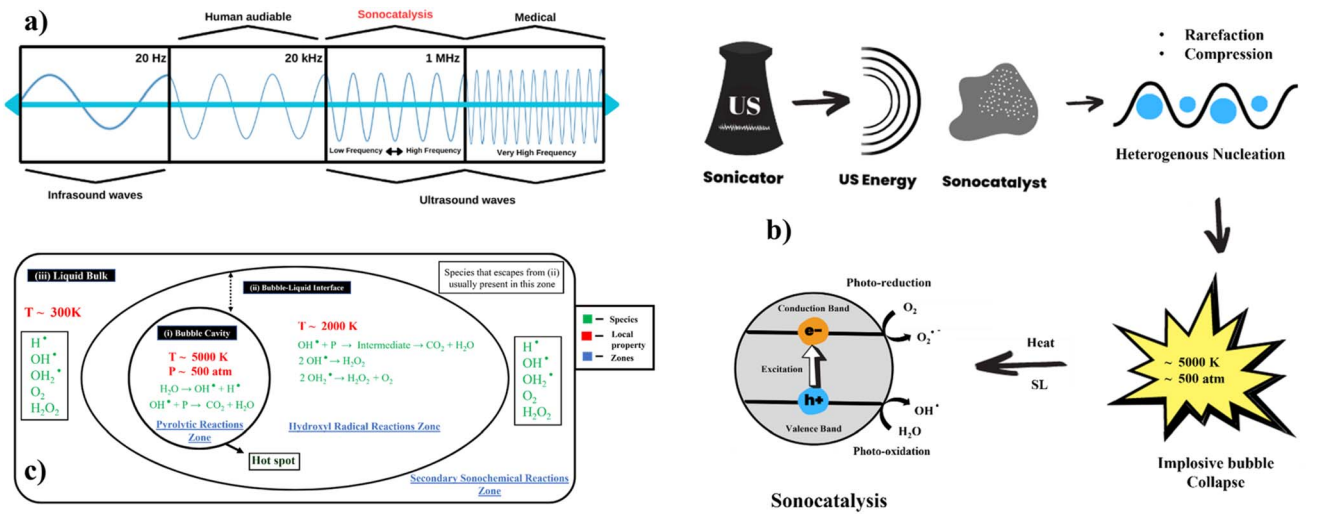

Fig. 2 (a) Pictorial illustration of frequency ranges of soundwaves, (b) mechanism of sonocatalytic process involving heterogenous nucleation, sonoluminescence, and thermal excitation and (c) implosive collapsed bubble's regional physical property (adopted from ref. 125).

Till today, three mechanisms have been proposed for semiconductor-assisted sonocatalysis and further research in this direction may leads to find new insights in sonochemistry.

2.1.1.1 Sonoluminescence mechanism. As mentioned earlier, sonoluminescence is one of the phenomena exhibited by acoustic cavitation. The luminescence encompasses a extent wavelength range (200–800 nm) and relatively high intensity.[38] When a sonocatalyst (semiconductor) is energized by the ultrasound irradiation to produce sonoluminesence (SL), the energy of the light emitted during SL is equal to or greater than the semiconductor bandgap, the electrons from (Valence Band) VB could be excited to (Conduction Band) CB. As a result, charge carriers (holes h^+ and electrons e^-) will be generated.[39]

2.1.1.2 Heterogenous nucleation mechanism. Unlike the sonoluminescene- and thermal-excitation mechanisms, the elucidation of the heterogeneous mechanism of sonocatalysis remains inadequate; only a few literature reviews addressed the heterogeneous process with limited context.[36,40,41] The significant stage in sonocatalysis is acoustic cavitation which is a non-linear process, and it can be breakdown into 3 stages; formation, growth, implosive collapse of bubble.[42] In this mechanism, the formation of bubbles (*i.e.* nucleation) occurred on the surface of the solid catalyst (sonocatalyst). In contrary to homogenous nucleation, the presence of heterogenous catalysts in the ultrasonic medium induces preferential nucleus development at the catalyst surface, which enhances bubbles birth or generation rate. Cavitation events occur in homogeneous nucleation *via* the temporary gas void (*i.e.* the combustion process), whereas heterogeneous nucleation events occur *via* crevices on the surface of the sonocatalyst as illustrated in Fig. 3a. The crevices and topological features of solid catalyst provides active sites which is advantageous for the cavity bubble nucleation and free radical formation.[41] Consequently, the excitation of electrons can be occurred through heat and light whereas in homogenous cavitation only pyrolysis and $OH^\bullet$ radical reaction occurs.[40] The growth rate of bubbles at the solid surface significantly influenced by three additional factors, (i) physicochemical properties of the sonocatalyst (morphology, particle size, topology, roughness and porosity) (ii) state of sonication (frequency, power and amount of liquid bulk) and (iii) environment (pH, temperature, pressure and type of adsorbed gas).

2.1.1.3 Thermal catalytic mechanism. The presence of localized high temperature caused by the implosive cavitation can possibly stimulate the thermal excitation of the semiconductor, resulting in the formation of electron–hole pairs. The radical generation and the degradation of the target pollutants occurred in the similar pathways as discussed in the previous sections. There are numerous studies on thermally assisted semiconductor catalysis are available in the literature and redirected for further studies.[43,44] The catalysts' improved efficiency could be attributable by the thermal catalytic activation.

2.2 Sonophotocatalysis (SPC)

Photocatalysis is a light-driven single-handed AOP where a semiconductor catalyst absorbs photons of suitable energy and generates electron–hole pairs on its fermi levels. These charge carriers migrate to the catalyst surface and initiate redox reactions that produce ROS ($HO^\bullet$, $O_2^\bullet$ and $HOO^\bullet$) capable of oxidize POPs.[45,46] This AOP technique is widely valued for utilizing light energy, avoiding harmful energy sources, and supporting complete degradation of POPs. The principles of photocatalysis form the foundation of sonophotocatalysis, which combines ultrasound and light energy to enhance pollutant elimination through synergistic effects. As far as hybrid oxidation processes are concerned, SPC is more efficient and convincing than sonocatalytic and photocatalytic processes for the generation of radicals. In typical sonophotocatalytic process, a nanocatalyst in the presence of ultrasound energy and light irradiation is used to destruct the pollutant. As a consequence of sonophotocatalysis, six AOP processes namely, sonolysis, photolysis, photocatalysis, sonocatalysis, sonophotolysis and sonophotocatalysis can occur simultaneously. In comparison to individual AOP technologies, h-AOP can be an effective tool for generating ROS at substantially higher yields.[31,47] The combination of sono- and photo-catalysis processes together demonstrate enhanced efficiency which may be due to several synergy effects as shown in Fig. 3b. The main aim of the h-AOPs is to reduce the operational cost and shorten the treatment duration.

The combination of various AOPs are responsible for the observed synergistic effect during the sonophotocatalytic mitigation of environmental contaminants. The following advantages are considered for the enhanced performance of the sonocatalytic and photocatalytic processes.

(i) The availability of light increases the production of oxidising species.

(ii) Sonolytic cleavage of water give rise to increase in oxidizing species.

(iii) Deaggregation induced by ultrasonic irradiation accelerates the mass transfer of the organic pollutant to the catalyst surface.

(iv) Limiting the recombination of electron–hole pairs.

(v) Turbulence caused by the US restrict the catalyst from aggregation.

(vi) Ultrasonic waves constantly clean the surface of the catalyst to stop pollutants and their intermediates from accumulation.

The adsorbed organic pollutant on the surface of sonophotocatalyst reacts with the ROS effected through photocatalytic process. Subsequently the transient implosion of cavity bubbles improvises the adsorption–desorption process, pyrolysis of water molecules and mass transfer. However, these h-AOPs sometimes can exhibit negative synergy effects.[48,49] S. Chakma and V. S. Moholkar studied the mechanistic issue of h-AOPs using pure and doped catalysts.[50] The authors discovered that shock waves decrease the possibility of dye–catalyst interaction, and the sonoluminescence light emitted during cavitation is also unable to activate the catalyst in the absence of external light. Thus, a negative synergy effect results; this demonstrates to achieve the synergy, the targeted design of the nanocatalyst facilitate to the nature of the pollutant and AOP processes are crucial.

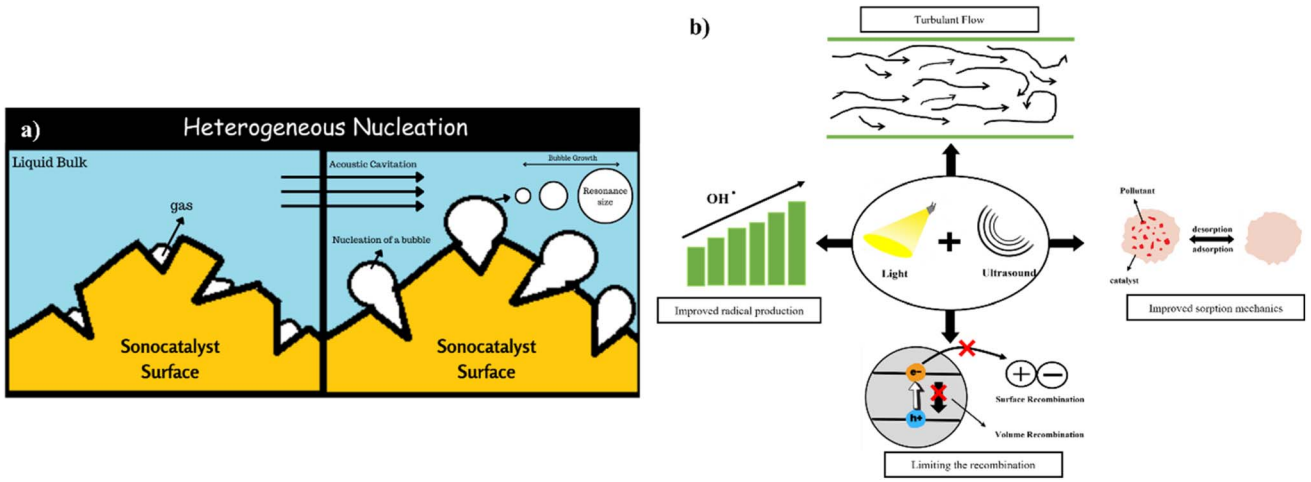

Fig. 3 (a) Heterogenous nucleation in solid surfaces of catalyst during sonocatalytic processes and (b) possible synergistic implications of sonophotocatalysis (sorption mechanics, internal turbulence, improved radical production and enhanced lifetime of carriers).

3. SDGs intented synthesis routes of MAX phases and MXene

When it comes to the synthesis routes for MXenes, several challenges arise in both the synthesis of their precursor (MAX) and the subsequent etching process. Among the available methods, the hydrofluoric acid (HF)-assisted route is widely regarded as the most efficient and straightforward approach to remove the A layer from 3D MAX phases. This is because HF can effectively oxidizes the A layer in MAX precursors, facilitating its disintegration and forming A fluoride (AF_3) {A = Al, Ga, P, Sn *etc.*,} as a by-product. However, the reagents involved in this process, as well as the resulting byproducts, exhibit highly hazardous properties to the environment. HF is a well-known strong acid with the ability to disintegrate most materials; it can permeate the skin and underlying tissues, posing severe risks to human health and safety.[51] Consequently, the traditional large-scale synthetic approach using HF could lead to significant environmental imbalances such as soil contamination, workplace safety, damage to biodiversity and bioaccumulation. To address these concerns, it is indispensable to explore strategies aimed at minimizing the harmful effects associated with HF-based synthesis. The adoption of safer chemicals and alternative routes for synthesizing MXenes from MAX phases is not only necessary but also highly desirable towards SDG.[52] In light of these challenges, this section discusses potential synthesis strategies to mitigate these adverse effects.

3.1 Optimizing MAX phase synthesis under reduced hazardous conditions

While analyzing the strategic routes for preparing MXenes, the top-down approach has proven to be more prominent which utilizes MAX phase precursors to produce MXenes.[53,54] Consequently, industries have adopted methods to synthesize MAX phases. However, concerns regarding environmental impact persist, as these procedures consume significant energy, with most methods requiring temperatures exceeding 1400 °C for the solid-state reaction to proceed.[55] To address these concerns, one viable solution is to harness renewable energy sources, such as solar energy, to power the reaction. This approach promotes sustainability and reduces environmental implications. By exploiting renewable energy, large-scale production of MAX phases can be achieved with a smaller carbon footprint and lower CO_2 emissions compared to processes reliant on fossil fuels. However, we believe that relying solely on renewable energy for MAX phase synthesis does not fully align with the SDGs.[56] A more sustainable method would involve synthesizing MAX phases at lower temperatures. This approach would not only minimize environmental pollution but also open up various pathways for broader research applications.

The preparation of MAX phases at lower temperatures can significantly reduce both economic and environmental impacts. For example, $Ti_3Al(Sn)C_2$ synthesized at low temperatures has introduced promising prospects for further research. Yang *et al.* discovered the inclusion of suitable "A" materials can effectively enhance oxidation resistance, as Sn can occupy Al sites, enabling successful synthesis at reduced temperatures, such as 900 °C.[57] Moreover, Z. Li *et al.* reported the synthesis of high-purity Ti_3AlC_2 MAX phases annealed at a low temperature of 700 °C using a high-power impulse magnetron sputtering method within just 90 minutes. The TEM analysis of the synthesized Ti_3AlC_2 MAX phases revealed superior growth with an intact morphology, as shown in Fig. 4a–d. Notably, the sequential stacking of Ti–C layers sandwiched between Al atom layers was precisely demonstrated by the atomic arrangement STEM micrograph of Ti_3AlC_2 grains (Fig. 4e). These novel process intensification studies in MAX phases have stimulated broader implications for other MAX phases.[58] Each synthesis route may vary depending on the objectives of the study, the precursors used and the conditions proposed for synthesis. However, some general aspects of adopting low-temperature MAX phase synthesis include economic feasibility, energy savings, reduced carbon emissions and more efficient utilization of available resources.

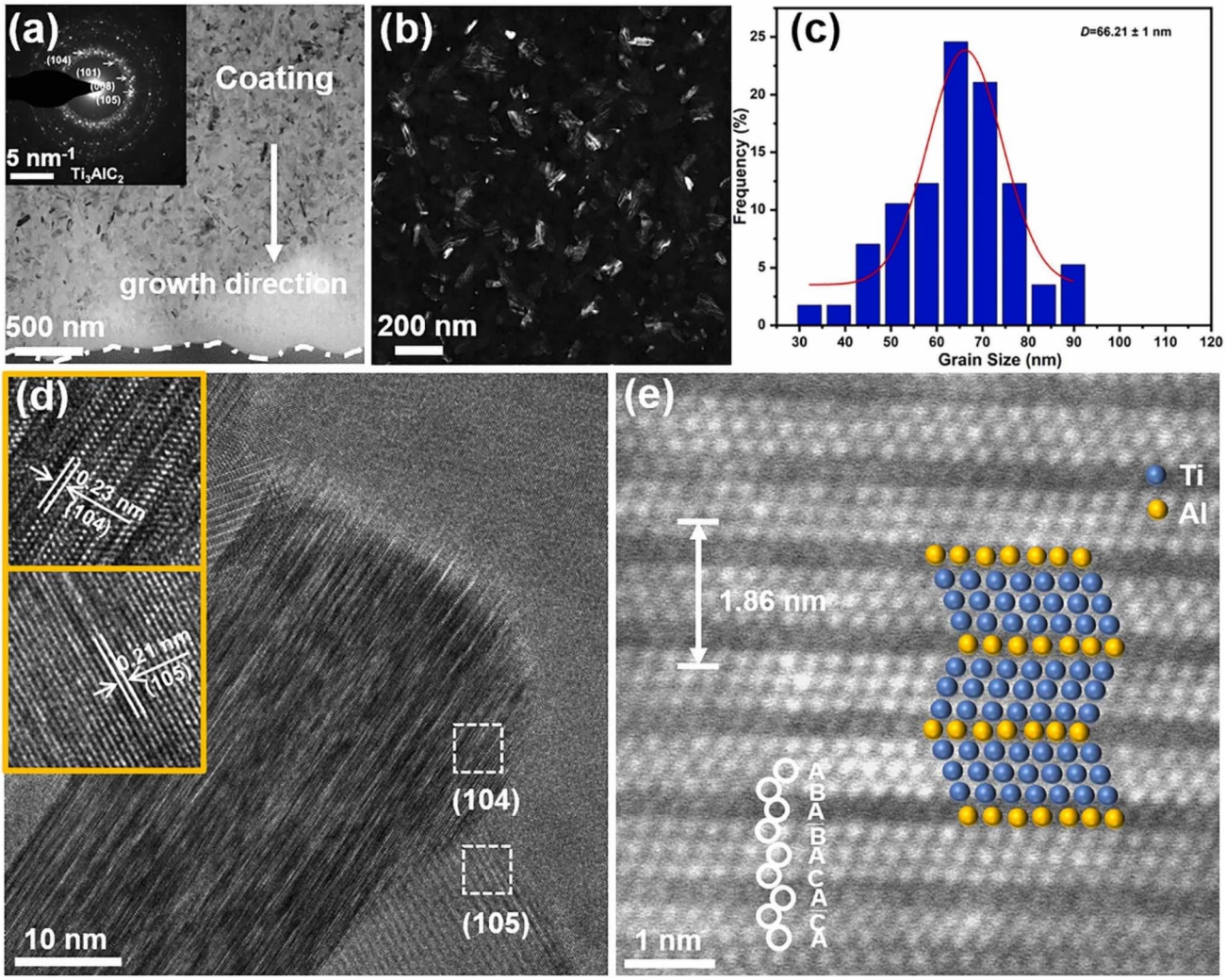

Fig. 4 (a and b) TEM micrographs of HiPIMS induced synthesis of Ti_3AlC_2 MAX phase, (c) grain size distributions calculated for (b) and (d) HRTEM micrographs of Ti_3AlC_2, (e) atomic arrangement STEM micrographs of Ti_3AlC_2 (reprinted with permission from Elsevier[58]).

On the other hand, adopting simpler strategies for preparing MAX phases such as utilizing milder reaction conditions and selective chemical condition, may significantly reduce the complexity of MAX synthesis while also lowering costs. Direct sol–gel chemical reactions (wet synthesis) are considered among the most effective and straightforward synthesis routes for various chemicals, as they offer tunability and size controllability by optimizing reaction conditions (*i.e.* solvent, reagents, templates and temperature). Additionally, adopting wet synthesis would result in MAX precursors to engage in atomic and molecular–level reactions, facilitating faster and more direct diffusion channels for the high-purity synthesis of MAX phases. In light of this, Sinclair *et al.* prepared a phosphorus-containing MAX phase, V_2PC, using a direct sol–gel method. The stoichiometrically optimized quantities of vanadium, phosphorus, and carbon sources were carefully mixed to form the V–P–C ternary phases treated at 140 °C. The resulting gel was then subjected to calcination to promote complete phase transformation and to eliminate impure secondary phases.[59] This direct strategy for preparing MAX phases *via* the sol–gel method enables safe and large-scale synthesis, reducing reliance on advanced/complex synthesis facilities such as CVD, milling, or plasma-based equipment. Beyond high-purity synthesis, the sol–gel method also offers chemical versatility that direct solid-state reactions cannot promote, such as size controllability and shape tunability. For example, Siebert *et al.* reported the straightforward synthesis of Cr_2GaC MAX phases through a sol–gel method utilizing nitrate salts of chromium and gallium, with chitosan as the carbon source.[60] The results from sol–gel-assisted MAX phases highlight the chemical versatility of sol–gel chemistry, with proposed reactions utilizing suitable carbon sources enabling various shape control possibilities, such as microspheres, hollow microspheres, and thin films.[61]

3.2 Etching of MAX phases using chemicals safer than HF

HF is a highly dangerous and toxic chemical commonly used during the etching of the "A" layer from MAX phases to prepare 2D MXene layers. However, exposure to HF poses significant health risks, including cardiovascular, pulmonary, and neuromuscular issues, especially when it penetrates the skin and

tissues through dermal contact. Even at a concentration of 0.04 ppm, HF can produce a pungent odor and fuming gas, while the PEL (Permissible Exposure Limit) is set at 3 ppm highlighting the HF potency even at such lower concentrations.[62,63] Consequently, exposure to HF fumes can lead to the deposition of highly toxic fluoride (F^-) ions in the lungs and internal organs, resulting in tissue and muscle damage/corrosion. As a result, the synthesis of MXenes should prioritize the use of less harmful chemicals compared to HF, thereby advancing this area of research toward achieving the SDGs.

Nevertheless, efforts have been made to synthesize MXenes from MAX phases without relying on hypertoxic HF acids or similar methods. For example, fluorine-free synthesis routes have emerged as a less-harmful pathway for etching the "A" layer from MAX phases, utilizing high concentrations of alkali hydroxides. T. Li *et al.* reported the high-purity synthesis of $Ti_3C_2T_x$ MXene with controllable terminal groups (T = OH and O) through a fluorine-free route. Interestingly, this alkali-assisted hydrothermal synthesis method was inspired by the Bayer process used for bauxite refining. The authors achieved up to 92% purity of $Ti_3C_2T_x$ MXene with excellent gravimetric capacitance.[64] The characteristic properties of fluorine-free synthesized MXene were analyzed using XPS and various micrographic tools, as shown in Fig. 5a–h. The survey XPS spectra of unetched MAX (Ti_3AlC_2) and etched MXene demonstrated a decline in Al orbitals indicating successful etching which was further confirmed by high-resolution XPS scans at the Al 2p orbital (Fig. 5e). SEM, TEM, and HAADF-STEM micrographs of $Ti_3C_2T_x$ flakes revealed characteristic accordion-like etched 2D MXene layers (Fig. 5f and g), and HAADF-STEM analysis showed the perfect alignment of Ti atomic positions, confirmed by non-uniform interlayer spacing (Fig. 5h). Alternatively, fluorine-free molten salts of Lewis acids with higher electrochemical redox potentials have been considered a more sustainable and effective method compared to the previous NaOH treatment.[65] These Lewis acid salts are regenerated upon the completion of the etching process, offering lower corrosivity towards the environment compared to HF.[66] Moreover, this synthesis method is adaptable to a broader range of MAX phases, whereas HF etching is predominantly selective for Al-based MAX precursors. By tweaking the electrochemical potential of the A-site in MAX phases and the corresponding Lewis acid etchant, targeted MXenes can be efficiently achieved

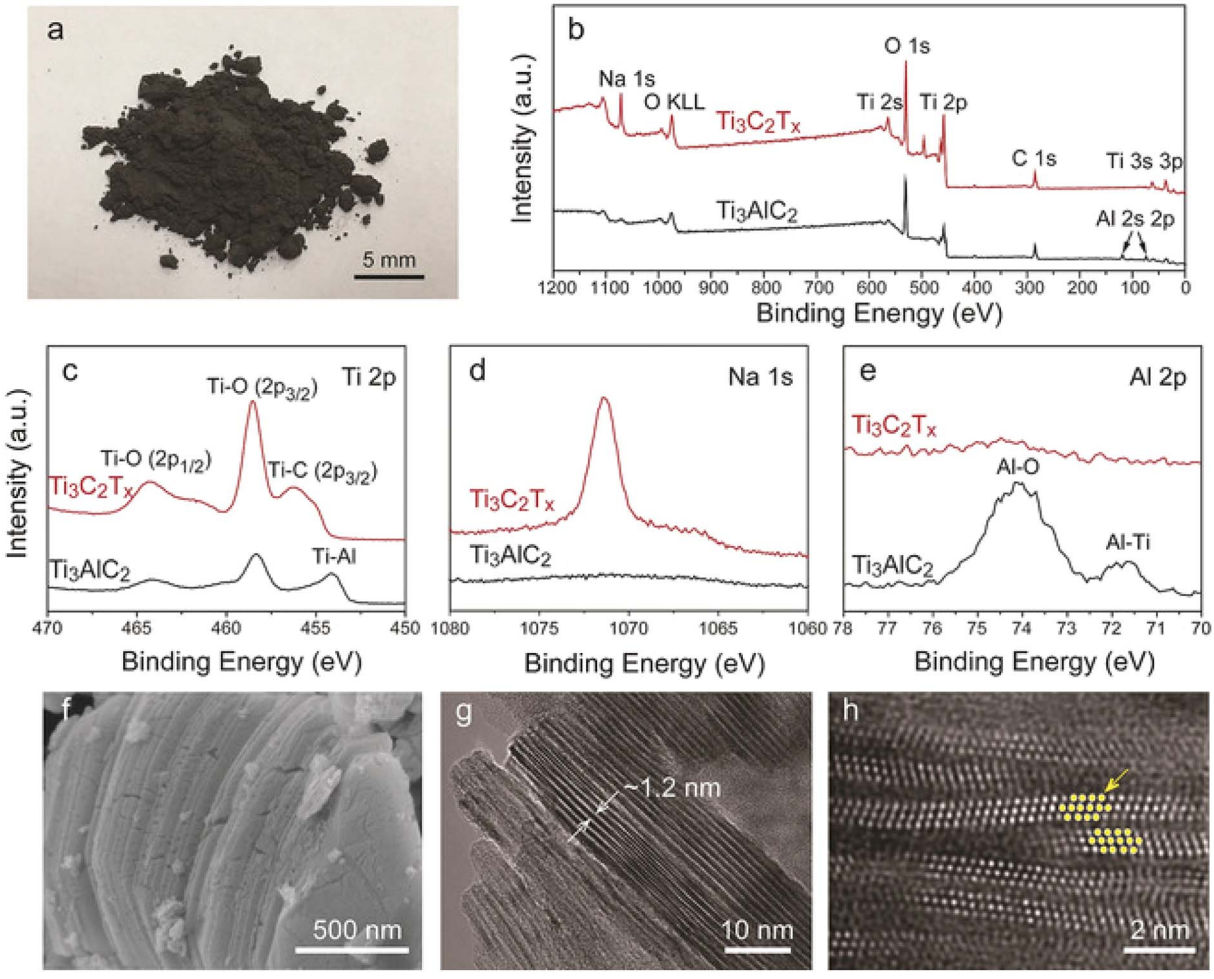

Fig. 5 (a) Digital photograph of $Ti_3C_2T_x$ powder (b) survey XPS scan of Ti_3AlC_2 MAX and Ti_3AlC_2 MX (c–e) high-resolution orbital XPS scan of Ti_3AlC_2 MAX and Ti_3AlC_2 MX (f–h) SEM, TEM and HAADF-STEM micrographs of Ti_3AlC_2 MX (reprinted with permission from John Wiley and Sons[126]).

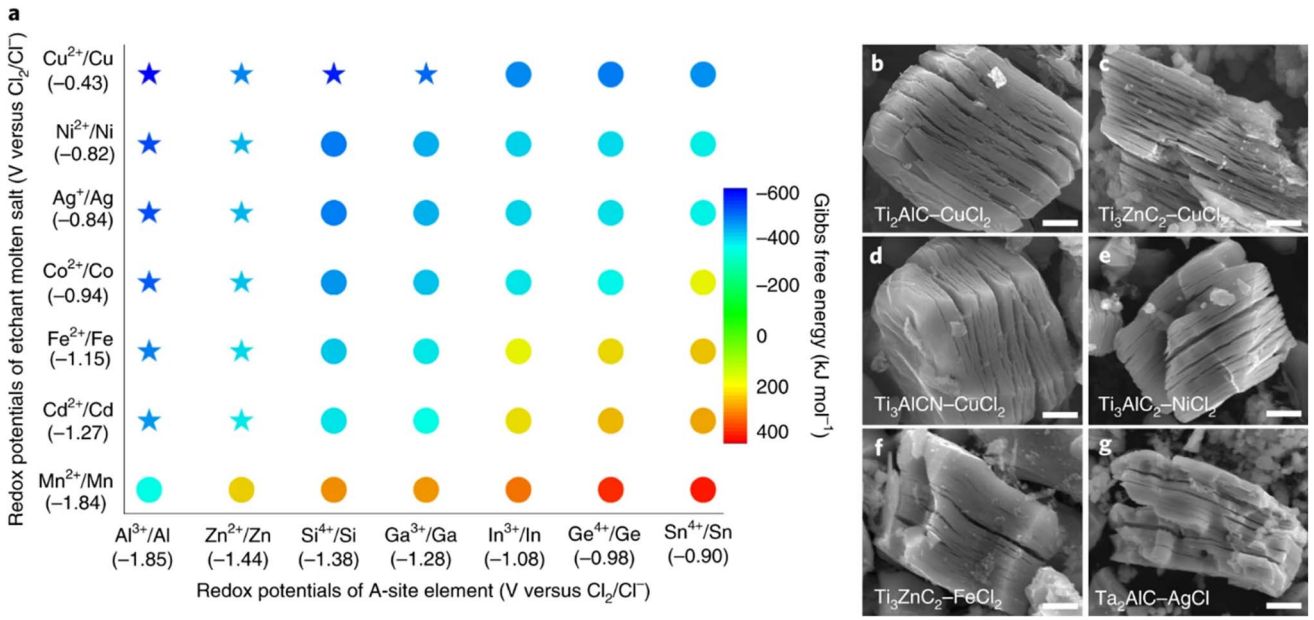

Fig. 6 (a) Redox potentials of A-sites in various MAX phases compared to molten salt (Cl^-) etchants of different cations, indicated based on Gibbs free energy. (b–g) SEM micrographs of various MXenes etched from MAX phases with different A-sites and corresponding Lewis acids (reprinted with permission from *Nature Materials*[127]).

with reduced treatment time and minimal temperature requirements, as shown in Fig. 6a. The use of various Lewis acid chloride salts directly influence the A-site in MAX phases. Fig. 6b–g depicts the book-like structure of etched MXenes derived from various MAX phases. Alternatively, Jiamin Zhu *et al.* developed a one-step A-etching method for MAX phases using the gas phase selective etching (GPSE) technique without relying on Lewis acids or molten salts. Pure 2D MXene phases were synthesized by etching various "A" elements such as Al, Si, and Sn through gas-induced functionalization in a sealed ampoule. Selective metal halides like $CuBr_2$ were heated above their decomposition temperature to produce etching gases that reacted with the 'A' layers in the MAX phases. The ampoule contained two temperature zones where by-products were separated in the lower zone and etched MXene formed in the higher zone as scheme mentioned eqn (1) and (2).[67] This method offers a cleaner pathway and better economic feasibility for scaling up MXene synthesis from MAX phases. Few other methods have been proposed focusing on the use of less harmful chemicals than HF for MXene etching. However, there remains a gap in fully utilizing sustainable resources such as US energy or solar energy to their full potential in the synthesis process of MXene.

$$2M_3AX_2 + 3I_{2(g)} \rightarrow 2M_3X_2 + 2AI_{3(g)} \quad (1)$$

$$2M_3X_2 + xI_{2(g)} \rightarrow 2M_3X_2I_x \quad (2)$$

3.3 Biocompatibility and toxicity of MXene in aquatic environment

The environmental biocompatibility and toxicity of MXenes, particularly titanium-based MXenes are increasingly recognized as a critical consideration for their catalytic use in wastewater treatment, especially in AOPs. Comparative studies on other MXenes such as Nb_2C, Mo_2C and V_2C have shown that toxicity levels vary significantly depending on the transition metal composition, metal ion leaching, M–X layer counts and surface terminals. For instance, Nb_2C exhibits relatively lower cytotoxicity compared to $Ti_3C_2T_x$, while Mo_2C and V_2C demonstrate higher oxidative stress potential rates and ROS generation.[68,69] Nevertheless, $Ti_3C_2T_x$ remains one of the more extensively studied MXene materials and shows moderate toxicity under controlled conditions, primarily due to its atomically thin edges and surface terminations (–OH, –F, –O) that can cause cell membrane damage at higher doses.[70] However, biocompatibility assessments disclose that when used at environmentally relevant concentrations or in immobilized forms (*e.g.*, lower concentrations, nanocomposites or supported membranes), MXene generally exhibits minimal cytotoxicity and is well tolerated.[71] For instance, *in vitro* toxicity analysis of $Ti_3C_2T_x$ nanosheets was performed on neural stem cells (NSCs) to evaluate their cytotoxicity.[72] Results indicated that $Ti_3C_2T_x$ nanosheets exhibited no adverse effects at a concentration of 12.5 μg mL^{-1} on NSCs and NSC-derived cells. However, increasing the dosage to 25 μg mL^{-1} led to significant cytotoxicity, primarily due to an elevated rate of apoptosis in the NSCs. Additionally, *in vivo* studies using the zebrafish (*Danio rerio*) model were conducted by Nasrallah *et al.* to assess the acute toxicity of $Ti_3C_2T_x$ nanosheets.[73] No mortality was observed up to a dosage of 50 μg mL^{-1}. Upon increasing the dosage to 100 μg mL^{-1} of nanosheets, the cumulative mortality rate of embryo model reached 21%. Based on *in vitro* and *in vivo* studies, the biocompatibility of MXenes is largely dose-dependent. However, standardized bio-dosage thresholds and regulatory guidelines are currently lacking due to the diverse composition and terminal functionalization of the MXene family (*e.g.*, Ti,

Mo, V, W, Nb, and others). Establishing uniform toxicity profiles and dosage limits is essential for advancing their safe and responsible application. Since MXene are more susceptible to environmental oxidation (oxide formation) and can decomposed into transition metal oxides, using immobilized forms instead of colloidal mixtures helps limit direct environmental leaching into aquatic systems.[74] Furthermore, lifecycle assessments and comprehensive ecotoxicological evaluation are essential to ensure long-term safety and regulatory compliance for their use in AOP-driven wastewater remediation.[75]

4. MXene for sonophotocatalytic degradation of various environmental toxins

4.1 Optical characteristics of MXene towards environmental application

For a material to be active in catalysis, especially in AOP-based catalysis, it should possess suitable electronic characteristics to participate in and promote the generation of ROS.[76] When it comes to MXenes, the pure $M_{n+1}X_n$ phases are inherently metallic in nature making them more effective as cocatalysts rather than as sole catalysts for heterogeneous catalysis reactions.[77] However, it is important to note that it is nearly impossible to prepare an ultra-pure phase of $M_{n+1}X_n$. During the etching process from MAX to MXene, surface functional groups such as F, OH, and O are introduced.[78] These functional groups and their concentrations, significantly alter the electronic properties of the resulting MXene, leading to a shift from metallic to semiconducting behavior. One of the main objectives in photocatalysis or sonocatalysis is the efficient utilization of energy for degradation. As a result of the functionalization of MXenes, they can be photoexcited when suitable energy is irradiated on their surface. However, as mentioned earlier even after surface functionalization, their semiconducting properties are not as strong as those of other materials like metal oxides. Many metal carbides possess bandgaps ranging from 0.9 to 2.1 eV, which are relatively low for effective visible light harvesting, making them less suitable as sole catalysts for light absorption and ROS generation. Consequently, a suitable material is required to enhance the visible light harvesting capability and improve the overall catalytic efficiency. For instance, Janani *et al.* reported a quaternary nanocomposite comprising Ti_3C_2/g-C_3N_4 with Fe_2WO_6/$BiIO_4$ for multifunctional applications.[79] Optical characterizations revealed that the

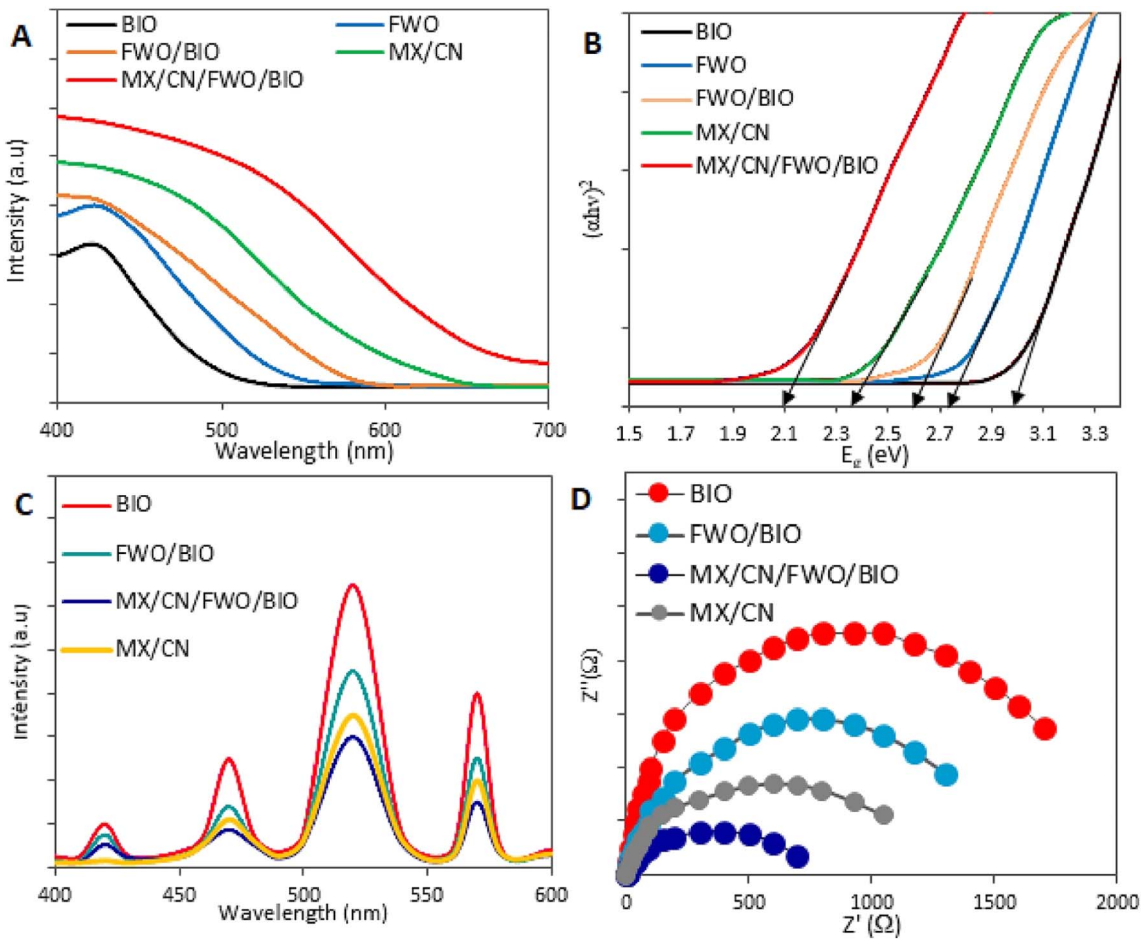

Fig. 7 Optical properties of synthesized nanocomposites along with its pure and binary counterparts. (A) UV-vis DRS specta (B) Tauc plot (C) steady state PL spectra (D) EIS spectra (reprinted with permission from Elsevier[79]).

bandgap of the resulting nanocomposite could be effectively optimized to the narrow visible light region. As shown in Fig. 7A and B, the inclusion of MXene in the quaternary nanocomposite shifted the band edges towards the 400–700 nm range. Consequently, the optical bandgap of pristine $BiIO_4$ shifted from 2.98 to 1.9 eV, resulting in improved visible-light harvesting. The steady-state PL analysis of the nanocomposites exhibited reduced luminescence, indicating a significant enhancement in the separation of charge carriers (Fig. 7C), which was further confirmed by EIS analysis. The quaternary nanocomposites demonstrated a notable reduction in electron mobility, directly illustrating the effective separation of electronic charge carriers (Fig. 7D). Moreover, similar results were reported by D. A. Upar *et al.*, fabricated a rational Z-scheme nanocomposite of g-C_3N_4–CdS–MXene for photo/electro/photoelectrocatalytic applications.[80] Due to the incomplete semiconducting properties and limited light absorption, MXene was employed as an electronic charge migrator. The charge migration was expected to occur from CdS to g-C_3N_4 *via* MXene, thereby providing an enhanced lifetime for photogenerated e^- and h^+ in an aqueous medium. Consequently, the production of ROS was increased, enhancing the kinetic rate to $k = 7.65 \times 10^{-3}$ s^{-1}, which led to superior photocatalytic efficiency in the degradation of methylene blue (MB) compared to pure CdS (1.6×10^{-4} s^{-1}). Various reports have suggested that MXene possesses excellent electronic charge migrator properties, indicating its potential in various heterojunction applications.

4.2 Surface features of MXene for enhanced cavitational events

Sonocatalysis prominently differs from photocatalysis in terms of stability and surface properties. In sonocatalysis, the primary mechanism of ROS production stems from the sonoluminescence excitation of the catalyst, as highlighted in numerous reviews over the years. However, when considering MXene, its 2D stacked interlayers and crevices within the accordion-like structure of $M_{n+1}X_n$ layers enhance acoustic cavitation, leading to increased intensity and the formation of transient bubbles as discussed in Section 2.1. The surface charges of MXene are also critical when employing it for environmental applications. In this context, B. M. Jun *et al.* studied the sonocatalytic degradation of two industrial dyes using $Ti_3C_2T_x$ as a sole sonocatalyst.[81] The results revealed that the MXene surfaces are negatively charged due to the inherent nature of metallic carbides, which facilitated better adsorption of methylene blue (MB) compared to acid blue (AB). In addition, some studies have conducted comprehensive analyses of the microstructure of MXene. Notably, S. Wang *et al.* discovered potential ionic tunnels within the MXene layers and the presence of extended interlayer spacings between neighboring $Ti_3C_2T_x$ sheets. As depicted in Fig. 8, cracks and crevices in the MXene nanostructure were clearly evidenced in atomically resolved annular dark field (ADF) micrographs.[82] This suggests that MXene-based materials are not only suitable for absorption-related applications but also for acoustic-related applications. The crevices,

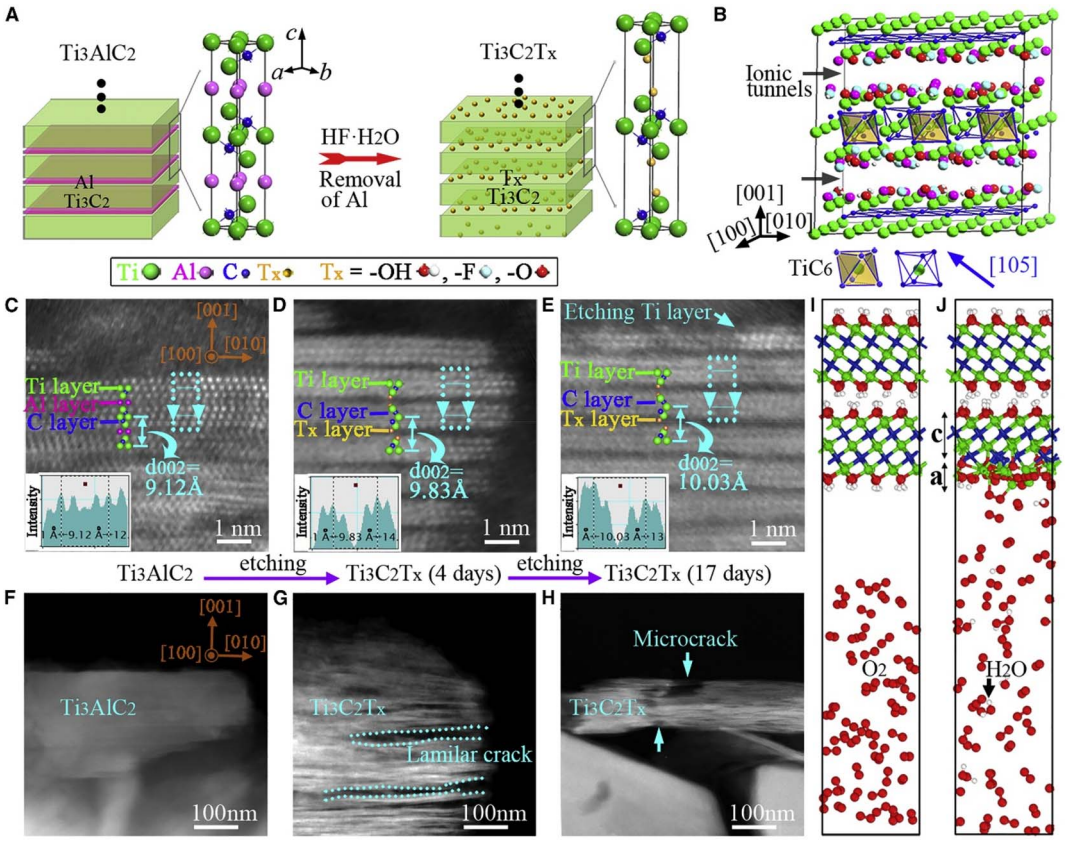

Fig. 8 (A and B) Scheme of $Ti_3C_2T_x$ synthesis (C–H) representation ADF micrographs of $Ti_3C_2T_x$ (I and J) MD simulation of $Ti_3C_2T_x$.

acting as neutral gas pockets within the nanostructure, facilitate heterogeneous nucleation, which further enhances the production of transient cavitation events.[83] However, the focused study on the interlayer distances of MXene and their effect on sonocatalytic performance remains unexplored to date.

4.3 Heterojunctional structures of MXene-based nanocatalysts

A sustainable and scalable approach in AOPs that fulfills the primary objective of catalytic decomposition of environmental contaminants involves the effective separation of charge carriers within the nanocatalyst's energy levels. The separation of charge carriers is directly proportional to the generation of ROS; the greater the separation, the longer the lifetime of the charge carriers, led to an enhanced generation of redox reactions and, consequently, more ROS. Therefore, it is essential for a supporting nanomaterial to form various heterojunctions within the nanostructures. Regarding MXene, it has been integrated into various heterojunctional structures, predominantly Z-scheme and S-scheme based. This section explores the potential heterojunctional structures derived from MXene in AOPs, with a particular focus on sonocatalysis and photocatalysis.

4.3.1 Z-scheme derived MXene nanocatalyst. The transfer of e^- from one band to another is considered a feasible and spontaneous method to enhance the separation time of h^+ and e^-.[84,85] Therefore, the Z-scheme is a significant type of heterojunction where electrons can migrate *via* an electron mediator, such as MXene. For example, Gao *et al.* reported a BiOBr/MXene/g-C_3N_4 Z-scheme for the photocatalytic removal of tetracycline (TC). The engineered heterojunction was characterized using various analytical tools to evaluate its extended lifetime and significance. As shown in Fig. 9a, steady-state photoluminescence (PL) demonstrated a notable decline in luminescence intensity, indicating that recombination is significantly restricted in the presence of Z-scheme migration. Moreover, the extended lifetime of charge carriers was confirmed by transient PL through fluorescence lifetime measurements (Fig. 9b). Additionally, the photocurrent

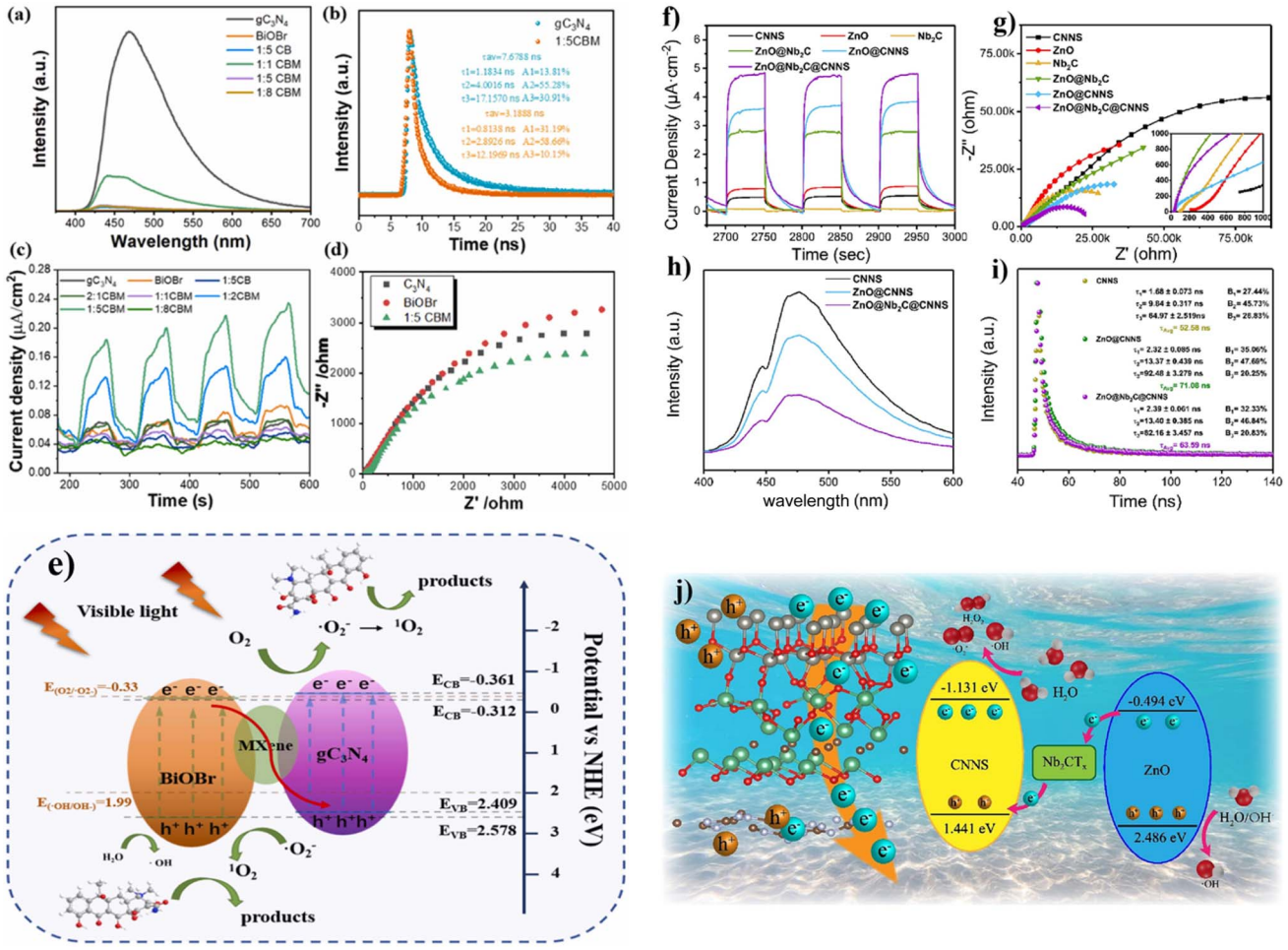

Fig. 9 (a and h) Steady state PL of BiOBr/MXene/g-C_3N_4, ZnO/Nb_2CT_x/g-C_3N_4 and its pristine counterparts (b and i) transient PL (c and f) transient photocurrent response (d and g) EIS Nyquist plot of the Z-scheme nanocomposites (e) photocatalytic mechanism of TC degradation in the presence of BiOBr/MXene/g-C_3N_4 (j) photocatalytic mechanism of EFX degradation in the presence of ZnO/Nb_2CT_x/g-C_3N_4 (reprinted with permission from Elsevier[86,87]).

response and Nyquist plots provided additional evidence of reduced mobility within individual bands and restricted recombination (Fig. 9c and d). The enhancement in TC degradation was attributed to the presence of oxygen vacancies and MXene quantum dots. However, a detailed analysis of the transpired changes occurring within the reused nanocomposite (8th cycle) in this context was lacking. Lastly, the authors illustrated the mechanism of TC photodegradation in the presence of the Z-scheme BiOBr/MXene/g-C_3N_4 composite, as shown in Fig. 9e.[86] The NHE potentials and bandgaps of each component in the composite support the formation of Z-scheme electron migration towards g-C_3N_4, facilitating the redox reaction of H_2O. Similarly, S. Li *et al.* fabricated a Z-scheme nanostructure of ZnO/Nb_2CT_x/g-C_3N_4 for the photocatalytic degradation of enrofloxacin (EFX). The catalyst achieved up to 98.2% elimination of EFX within 40 minutes of light irradiation, attributed to the efficient charge separation mechanism facilitated by Nb_2CT_x MXene, which minimized recombination. The enhanced separation efficiency was supported by photocurrent studies and the Nyquist plot of the synthesized Z-scheme nanocatalyst.[87] Notably, both steady-state PL and transient PL demonstrated that the Z-scheme effectively enhanced the lifetime of charge carriers, as shown in Fig. 9h and i. Ultimately, the degradation mechanism comprising charge migration pathway was illustrated in Fig. 9j.

4.3.2 S-scheme derived MXene nanocatalyst. The Schottky junction-based charge migration involves separating electrons from the CB of one semiconductor to another, thereby limiting recombination.[88–90] Given MXene's optical properties, which include limited light absorption and excellent electrical conductivity, electron migration from the CB is easily facilitated. Due to these properties, various nanocatalyst combinations have been reported as suitable S-scheme-based nanocatalysts for environmental applications (Table 1). For example, D. E. Lee *et al.* synthesized a novel CoAl layered double hydroxide supported by TiO_2/Ti_3C_2 MXene for the sustainable elimination of Diclofenac (DFC), RhB, and Indigo Carmine (IDC). The nanocomposites feature 2D/0D/3D contacts with TiO_2 engineered for maximum light absorption. Consequently, e^- excited by light energy were migrated to the Ti_3C_2 MXene CB by restricting recombination. Additionally, photocatalytic degradation experiments revealed that the nanocomposites achieved 75%, 69%, and 78% removal of DFC, RhB, and IDC, respectively.[91] However, the efficiency was higher under mild conditions suggesting a narrow pH activity range, which may be attributed to the oxidation of layered double hydroxides under strongly acidic or basic environments. The coupling Ti_3C_2 MXene in the nanocomposite structure enabled the Schottky junction, thereby separating electrons and reducing recombination, as illustrated in Fig. 10a. Similarly, C. Yao *et al.* fabricated a 2D/2D Schottky nanocatalyst using α-Fe_2O_3 supported with single-layered Ti_3C_2 MXene (SL-TIC) for PMS-activated degradation of tetracycline (TC). It was revealed that the α-Fe_2O_3/SL-TIC/PMS system achieved up to 17.3- and 5.6-fold enhanced degradation of TC compared to α-Fe_2O_3 and α-Fe_2O_3/PMS, respectively. This drastic enhancement is attributed to the photoexcited electrons migrating to the CB of MXene, thereby allowing the h^+ in the VB of α-Fe_2O_3 to favorably activate PMS, generating $SO_4^{\cdot 2-}$ radicals. Consequently, the backflow of e^- to the VB was restricted, and the photoreduction of H_2O subsequently resulted in the generation of ROS to degrade TC, as illustrated in Fig. 10b.[92]

The utilization of MXene in multifaceted nanocomposites, such as quaternary composites, has increased in recent years due to its electron sink properties, which effectively enhance the lifetime of charge carriers through migration across multiple counterparts. These advanced catalysts are expected to deliver improved degradation efficiency and higher pollutant removal rates. In this context, Liu *et al.* developed a quaternary nanocomposite comprising BiOBr/Bi_2MoO_6 supported by oxygen-functionalized Ti_3C_2 with montmorillonite (BBTM) for the decomposition of levofloxacin under visible-light photocatalysis. The BBTM photocatalyst demonstrated exceptional photoactivity, achieving 99% removal of levofloxacin (LEV) within 120 minutes. This remarkable performance was attributed to the restricted backflow of electrons from the CB of BiOBr/Bi_2MoO_6 to its VB. Furthermore, the work function (E_f) of transpired nanocomposites supported the favorable bending of band edges, facilitating electron migration to Ti_3C_2/montmorillonite.[93] The schematic illustration of the photocatalytic mechanism of the quaternary nanocomposite for LEV degradation is depicted in Fig. 10c. This work underscores the versatility of MXene in nanocomposites and its feasibility in S-scheme-based photocatalysis.

4.3.3 Other unique heterojunctions. Among the heterojunctions, Type II and Type I junctions are quite common and were therefore intentionally excluded from our focus. However, in recent years, several new types of heterojunctions have been proposed for MXene-derived nanocatalysts, specifically for environmental remediation and related applications. Y. Wu *et al.* fabricated a unique heterojunction photocatalyst based on MXene and termed it as "M-scheme," for the photoreduction of CO_2. The photocatalyst consisted of two metal oxides (CeO_2 and TiO_2) supported by Ti_3C_2 to facilitate efficient charge separation. Consequently, the nanocatalyst was synthesized through chemical etching of the MAX phase (Ti_3AlC_2), followed by loading the metal oxides onto the surface of Ti_3C_2 using a hydrothermal route. The results from the photoreduction of CO_2 showed a selectivity of up to 70.6% with 0.22 μmol h^{-1} upon using 50 mg of the fabricated nanocatalyst.[94] The superior photocatalytic activity was attributed to the photogenerated charge migration of e^- from the metal oxides to the CB of MXene, and the corresponding mechanism was labeled as the M-scheme, as shown in Fig. 11a. In a similar context, Z. Yao *et al.* proposed a new scheme called the "r-scheme" and used Ti_3C_2 with MoS_2 as an effective photocatalyst for energy and environmental applications. The fabricated Ti_3C_2/MoS_2 nanocatalyst demonstrated 97.4% removal of methyl orange and 380.2 μmol h^{-1} g^{-1} of H_2 evolution under visible light. The enhanced degradation and H_2 evolution were ascribed to the electron sink properties of Ti_3C_2, which acted as a Schottky junction to migrate electrons from MoS_2, thereby reducing spatial recombination during photocatalysis. However, the authors described the mechanism as the r-scheme, which

Table 1 List of MXene based nanoarchitectures for the degradation of various organic pollutants

S. no.	Catalyst	Pollutant	Degradation (%)	Catalytic process	Reactor	Intermediate analysis	Ref.
1	$Ni_2Mg_{4-x}S_4$@$Ti_3C_2T_x$	BPA	92%	Sonophotocatalysis	970 kHz, 400 W US and 250 W LED lamp	Yes	128
2	$Ti_3C_2T_x$@TiO_2/WS_2	TC	98.9%	Sonophotocatalysis	—	No	98
3	N–TiO_2/$Ti_3C_2T_x$	Rhodamine B Methylene blue Levofloxacin *p*-Nitrophenol	98.1% 88.4% 65.9% 44.6%	Sonophotocatalysis	53 kHz, 35 kHz US and xenon lamp 500 W	No	129
4	$Ti_3C_2T_x$/MIL-101 (Cr)	Sulfadiazine Acetaminophen	96.1% 99.3%	Sonocatalysis	40 kHz, 180 W US	No	105
5	$Ti_3C_2T_x$/MIL-125 (Ti)	Rhodamine B Microplastics	~90% ~75%	Sonocatalysis	35 kHz, 150 W US	No	130
6	Single layered and multilayered MXene	Diclofenac Verapamil	85.1% and 81.8% 100%	Sonocatalysis	570 kHz, 180 W	No	102
7	$CoTiO_3$ –$Ti_3C_2T_x$	Bisphenol A	96.9%	Sonocatalysis	970 kHz, 300 W	No	131
8	$Ti_3C_2T_x$	Methylene blue	90%	Sonocatalysis	970 kHz, 180 W	No	81
9	$Bi_2O_2CO_3$/Ti_3C_2/g-C_3N_4	BPA	80.2%	Multi-frequency sonophotocatalysis	20 + 40 + 80 kHz US, blue LED (457 nm, 12 W)	Yes	99
10	ZnO/Nb_2CT_x/g-C_3N_4	Enrofloxacin	98.2%	Photocatalysis	Xenon lamp	Yes	87
11	Boron nitride/Ti_3C_2/$ZnIn_2S_4$	4-Chlorophenol	90%	Photocatalysis	Xenon lamp, 300 W	No	132
12	CoAl (LDH)/TiO_2/Ti_3C_2	Diclofenac Rhodamine B Indigo carmine	75% 69% 78%	Photocatalysis	Xenon lamp, 150 W	Yes (investigated for DFC)	91
13	a-Fe_2O_3/single-layered Ti_3C_2	Tetracycline	99%	Photocatalysis	Sunlight	No	92
14	Ti_3C_2/MoS_2	Methyl orange	97%	Photocatalysis	Xenon lamp	No	95
15	TiO_2/$Ti_3C_2T_x$	Carbamazepine	98.67%	Photocatalysis	Solar simulator light & UV light	Yes	134
16	$CuFe_2O_4$/$Ti_3C_2T_x$	Sulfamethazine	60%	Photocatalysis	Xenon lamp, 300 W	Yes	135
17	Gd, Sn doped $BiFeO_3$/$Ti_3C_2T_x$	Congo red	100%	Photocatalysis	400–700 nm, Xe lamp, 300 W	No	136
18	g-C_3N_4/$Ti_3C_2T_x$/black phosphorus	Ciprofloxacin	99% within 60 min	Photocatalysis	420 nm cut off filter, Xe lamp, 300 W	Yes	137
19	$Ti_3C_2T_x$/MoS_2	Ranitidine	88.4%	Photocatalysis	LED lamp, 25 W	No	138
20	$Ti_3C_2T_x$/$BiFeO_3$	Congo red & acetophenone	100% & 100%	Photocatalysis	Xenon lamp, 300 W	No	139
21	$Ti_3C_2T_x$ – oxides	Methylene blue	89% on UV & 95% on vis	Photocatalysis	—	No	140
22	Gd doped V_2O_5/$Ti_3C_2T_x$	Methylene blue	92%	Photocatalysis	—	No	141
23	Bi_2WO_6/Nb_2CT_x	Methylene blue Rhodamine B Tetracycline hydrochloride	99.8% 92.7% 83.1%	Photocatalysis	(λ > 420 nm), xenon lamp, 500 W	No	96
24	$BiOIO_3$/Ti_3C_2	Tetracycline hydrochloride Diclofenac sodium Levofloxacin hydrochloride 4-Nitrophenol	93.4% 87.6% 77.4% 43.3%	Photocatalysis	Xe lamp, 500 W	No	142
25	Fe_2O_3/$Ti_3C_2T_x$	Rhodamine B	91%	Photocatalysis	(λ > 420 nm), Xe lamp, 500 W	No	143
26	Holey-Ti_3C_2/Ag/AgBr	Methyl orange	99%	Photocatalysis	(λ > 420 nm)	No	144

Table 1 (*Contd.*)

S. no.	Catalyst	Pollutant	Degradation (%)	Catalytic process	Reactor	Intermediate analysis	Ref.
27	N–Ti_3C_2	Methyl orange	98.73% within 20 min	Photocatalysis	Mercury lamp, 1000 W	No	145
28	Defect Ti_3C_2/$BiOIO_3$	Methyl orange	95.2% in 30 min	Photocatalysis	Xenon lamp, 300 W	No	146
29	g-C_3N_4/TiO_2/Ti_3C_2	Methyl orange	93.1%	Photocatalysis	Xenon lamp, 300 W	No	147
30	BiOI/Ti_3C_2	Rhodamine B	99.8%	Photocatalysis	Xenon lamp, 300 W	No	148
31	Urchin-like TiO_2/$Ti_3C_2O_x$	Levofloxacin	7.7 folds higher than pure TiO_2	Photocatalysis	8 W LED lamp	Yes	149
32	g-C_3N_4/BiOBr/MXene	Tetracycline hydrochloride	99%	Photocatalysis	Xe lamp, 300 W	Yes	86
33	ZnO/$Ti_3C_2T_x$	Formaldehyde Methanol Acetone	83% 84% 80%	Photocatalysis	125 W mercury lamp or 300 xenon lamp	No	97
34	BiOCl/$Ti_3C_2T_x$	Ciprofloxacin	90% in 30 min	Photocatalysis	Not mentioned	No	150
35	Bi_2WO_6–Ti_3C_2–$SnNb_2O_6$	Tetracycline hydrochloride	84%	Photocatalysis	Xenon lamp, 300 W	Yes	151
36	ZnS/$Ti_3C_2T_x$	Tetracycline hydrochloride	96%	Photocatalysis	Metal halide lamp, 500 W	No	152
37	C/Ti_3C_2/(001)TiO_2	Tetracycline	92.3%	Photocatalysis	Xenon lamp, 350 W	Yes	153
38	TiO_2/$Ti_3C_2T_x$/AgI	Tetracycline hydrochloride	97%	Photocatalysis	Xenon lamp, 350 W	Yes	154
39	$Bi_2O_2CO_3$/Ti_3C_2	Tetracycline	81%	Photocatalysis	Xenon lamp, 300 W (420–780 nm)	Yes	155
40	Ti_3C_2–SO_3H/g-C_3N_4	Tetracycline	75%	Photocatalysis	Xenon lamp, 35 W	Yes	156
41	V_2C/g-C_3N_4	Methyl orange	94%	Photocatalysis	Xenon lamp, 300 W	No	157
42	$CdTiO_3$/Ti_3C_2	Rhodamine B	85.8% in 180 min	Photocatalysis	Xenon lamp, 200 W	No	158
43	BiOBr/Bi_2MoO_6/Ti_3C_2/MMT_{ex} (MMT_{ex} = exfoliated montmorillonite)	Norfloxacin Ciprofloxacin Ofloxacin Levofloxacin	91% 90% 97% 99%	Photocatalysis	Xenon lamp, 500 W	Yes (investigated for levofloxacin)	93
44	g-C_3N_4/Ti_2C_3 derived	Rhodamine B Tetracycline	97.2% 86%	Photocatalysis	Xenon lamp, 270 W	Yes	159

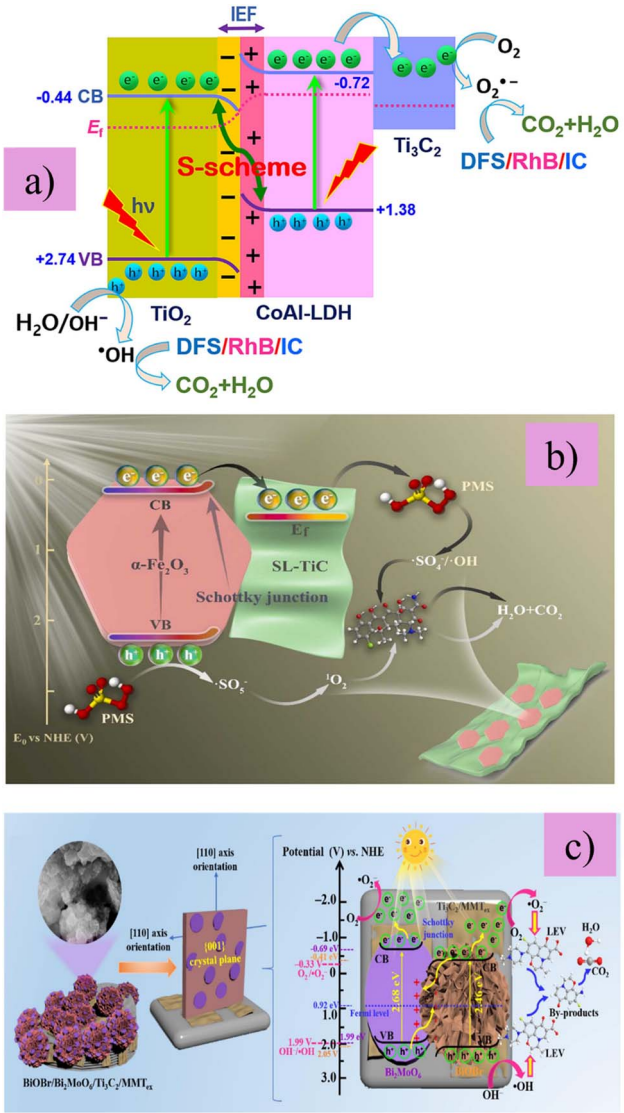

Fig. 10 Schematic representation of plausible S-scheme mechanism of photocatalytic degradation of targeted pollutants using (a) CoAl-LDH/TiO_2/Ti_3C_2 (b) α-Fe_2O_3/Ti_3C_2 (c) BiOBr/Bi_2MoO_6/Ti_3C_2/MMT_{ex} (reprinted with permission from Elsevier[91–93]).

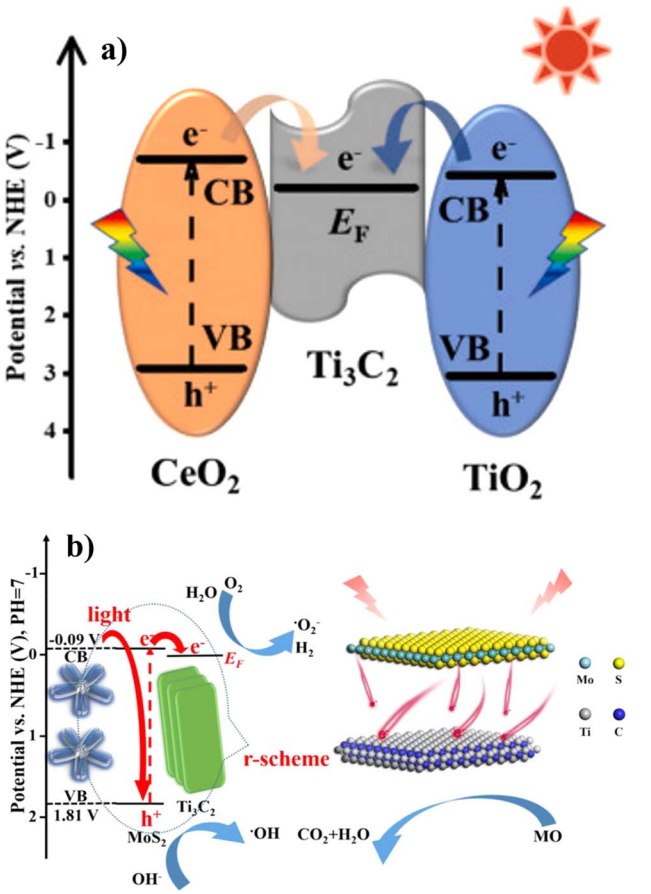

Fig. 11 Schematic representation of photocatalytic mechanism of (a) CeO_2/Ti_3C_2/TiO_2 – M-scheme (b) Ti_3C_2/MoS_2 – r-scheme (reprinted with permission from Elsevier[94]).

should be more appropriately labelled as the S-scheme based on the experimental results, as shown in Fig. 11b.[95]

4.4 Recent advancements on MXene assisted sonophotocatalysis

The key characteristics of MXenes are beneficial to h-AOPs which includes (i) terminal functional groups that can result in strong connectivity to various counterparts; (ii) uniform porosity distribution and large surface area for active redox chemical reactions; (iii) metallic conductivity of MXene that enhances charge migration throughout extended structure; (iv) acts as Schottky junction to recombinations; and (v) hydrophilicity of MXene facilitates the adsorption of aqueous pollutants with suitable surface charges. Over the past few years, researchers have shown more interests in preparing new class of MXenes with alternative metal centres to explore the role of catalysts in the AOP.[96,97] The present section summarizes the recent findings and advancements in the MXene-based catalysts used in sono–photo-catalytic degradation technologies. Most of the research works are focused on photocatalysis only, however other AOPs also explored as years progressing. Nevertheless, we believe that previous reviews related to the context of our study have lacked in presenting comprehensive data on MXene-assisted h-AOP. Therefore, Table 1 summarises recent works and findings from the MXene-based catalysts in the field of AOPs (sono–photo-catalysis).

In this regard, Vigneshwaran *et al.* reported the sonophotocatalytic removal of BPA using a novel bimetallic nanocomposite tethered with MXene ($Ti_3C_2T_x$).[128] They fabricated MXene as a co-catalyst with $Ni_2Mg_{4-x}S_4$ (NMS), and the nanocomposite was synthesized *via* a simple hydrothermal method, as shown in Fig. 12a. The NMS@$Ti_3C_2T_x$ exhibited superior catalytic activity under various AOP conditions (Fig. 12b). Notably, the highest degradation efficiency was achieved with h-AOP (sonophotocatalysis), resulting in a BPA degradation efficacy of approximately 91%. Furthermore, the authors employed the MXene nanocomposite to evaluate its catalytic potential against various major environmental pollutants. Interestingly,

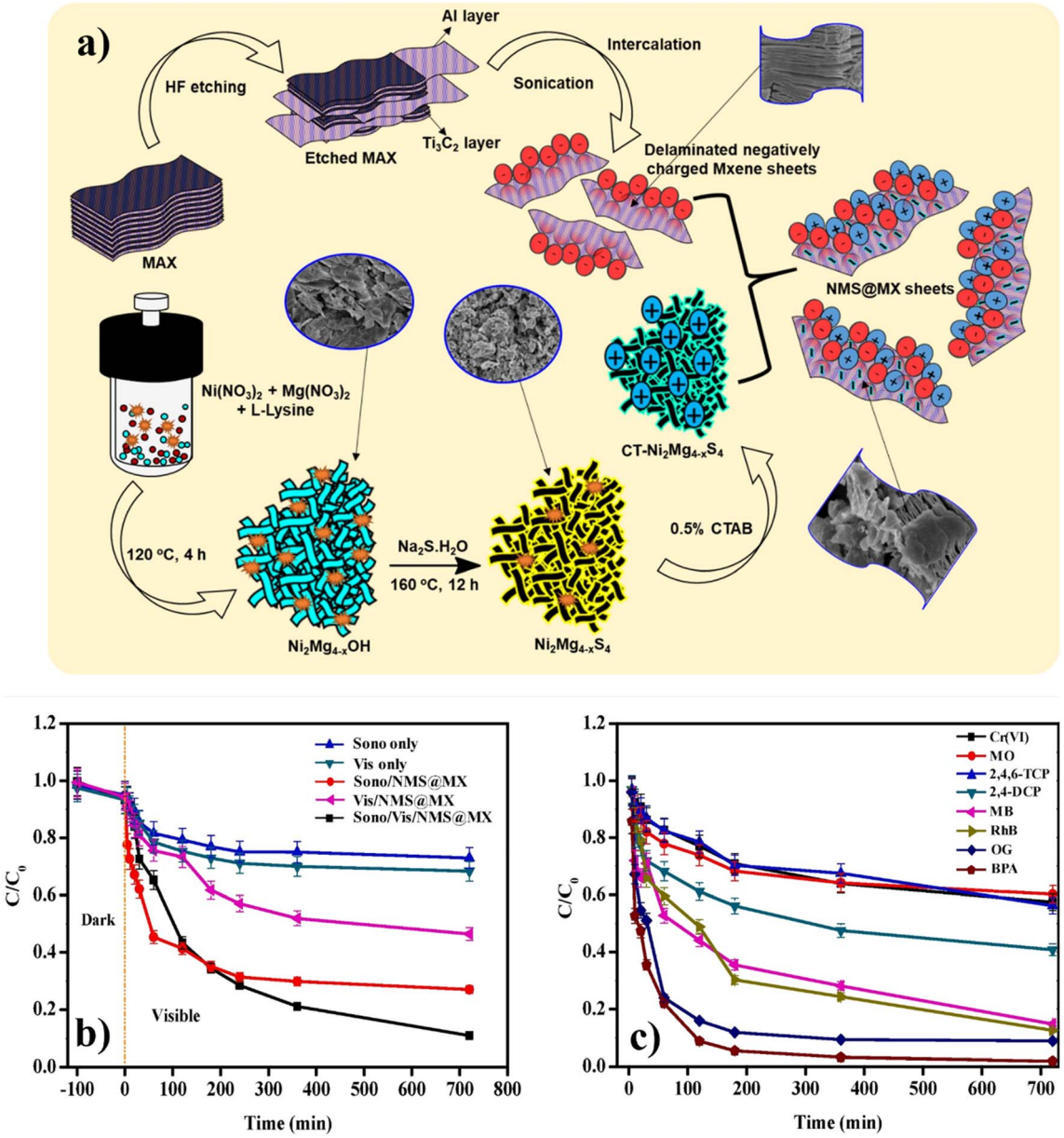

Fig. 12 (a) Representative scheme of $Ni_2Mg_{4-x}S_4/Ti_3C_2$ bimetallic nanocomposite. (b) Time-dependent degradation efficiency of various AOP/h-AOP processes, including sonolysis, photolysis, sonocatalysis, photocatalysis, and sonophotocatalysis. (c) Degradation efficiency of $Ni_2Mg_{4-x}S_4/Ti_3C_2$ bimetallic nanocomposite against various environmental contaminants (reprinted with permission from Elsevier[128]).

the nanocomposite demonstrated significant catalytic potential for environmental applications, including the removal of Cr(IV), methyl orange, chlorophenols, and azo dyes (Fig. 12c). Consequently, this study highlighted the broad applicability of MXene-based nanocatalysts in addressing a wide range of environmental toxins. In alignment with the MXene-based catalyst for h-AOP, Ranjith *et al.* investigated the decomposition efficiency of tetracycline (TC) using WS_2-intercalated $Ti_3C_2T_x$@TiO_2 nanostructure under sonophotocatalytic conditions. The nanostructure was fabricated through HF etching followed by hydrothermal treatment to produce $Ti_3C_2T_x$@TiO_2-WS_2, as illustrated in Fig. 13a. Although the authors did not disclose specific working conditions for the sonophotocatalytic environment, such as ultrasound frequency and light intensity, their experimental results demonstrated that the $Ti_3C_2T_x$@TiO_2-WS_2 nanostructure significantly enhanced TC decomposition efficiency under sonophotocatalysis.[98] The synergistic effect of h-AOP resulted in a decomposition rate of 0.0341 min^{-1} for sonophotocatalysis, compared to 0.0078 min^{-1} for sonocatalysis and 0.0171 min^{-1} for photocatalysis, as shown in Fig. 13b–d. This study further highlights the versatility of MXene-based nanostructures for h-AOP applications in water treatment. Moreover, similar results were reported by Ding *et al.*, utilized nitrogen-doped TiO_2 supported by Ti_3C_2 MXene for the removal of a wide range of environmental contaminants. They demonstrated enhanced removal

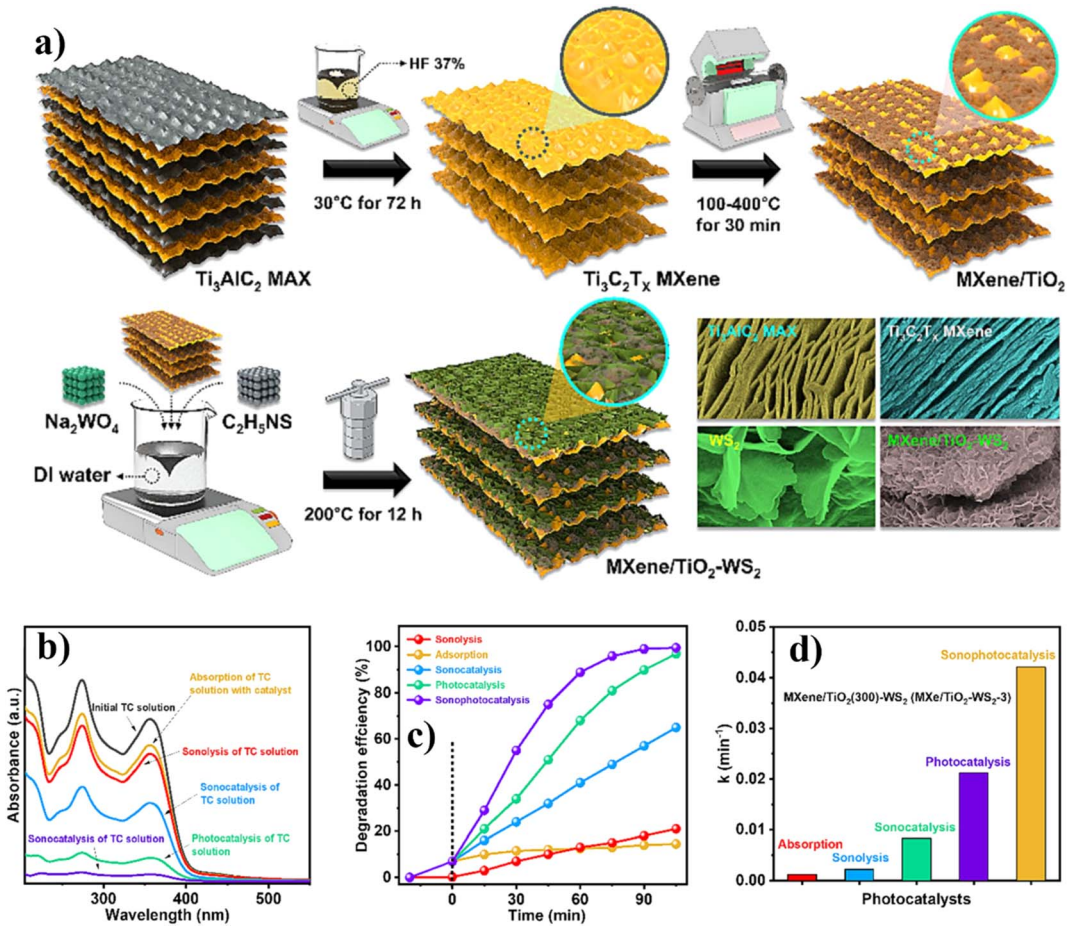

Fig. 13 (a) Schematic illustration of $Ti_3C_2T_x$@TiO_2-WS_2 nanostructure synthesis. (b) UV-vis spectra of TC degradation under various AOP and h-AOP conditions. (c & d) Degradation efficiency and rate comparison of different AOPs using $Ti_3C_2T_x$@TiO_2-WS_2.

efficiencies of various pollutants, including Rhodamine B, methylene blue, levofloxacin, and *p*-nitrophenol, under sonophotocatalytic (h-AOP) conditions.

The toxicity of intermediates formed during the degradation process was analysed since these by-products may sometimes be more harmful than the parent compounds and persist in the environment for long time. Therefore, the intermediates identified in the degradation pathway of organic pollutants should be carefully assess for their toxicity and biosafety. In this regard, Sheik Moideen Thaha and Sathishkumar reported the fragmentation of intermediates during the degradation of BPA using $Bi_2O_2CO_3/Ti_3C_2/g\text{-}C_3N_4$ nanocomposites under the sonophotocatalytic environment.[99] The toxicity of these intermediates were evaluated using Toxicity Estimation Software Tool (T.E.S.T v.5.1.2), and tested against models like fathead minnow, *T. pyriformis*, and *D. magna*. The inhibitory growth concentration (IGC50) and lethal concentration (LC50) values of the intermediates were higher than those of BPA, demonstrating that the degradation products were less toxic. Similar findings have also been reported by Qiang Li *et al.* and S. Birudukota *et al.*[100,101]

Although numerous efforts have been initiated in exploring MXene as a co-catalyst, only a few studies have thoroughly examined the effects of various parameters, such as the number of layers, interlayer distances and terminal functionalizations, in light to environmental applications. In this context, Sewoon Kim *et al.* studied the degradation of diclofenac and verapamil using single and multi-layered MXene as a sonocatalyst. The authors discovered that MXene solid surfaces improved $OH^{\bullet}$ radical production by 48.8% for single-layered MX and 59.8% for multi-layered MX.[102] The observed results indicating the remarkable hydrophilicity property possessed by the MXene surface. In addition, MXene has a high electron content (sink) and a negative charge in its natural state and verapamil has a positive charge, which resulted 100% degradation, whereas diclofenac has shown only to a lesser extent. This is due to the pollutant's electrostatic attraction to the surface of MXene, which is extended by the terminal functional groups (F, O, –OH, –COOH) presents in the MXene.

Despite adsorption-based AOPs are not the primary focus of our current review, it is important to note that nearly all AOPs include an initial rest/dark/adsorption–desorption time without energy irradiation to establish equilibrium between oxidant and contaminant.[103] Therefore, the adsorption properties of MXene are also a significant parameter to investigate in order to optimize the nanocatalyst. S. Kim *et al.* investigated the adsorption performance of sonicated MXene ($Ti_3C_2T_x$) with various pharmaceutical compounds, and their findings confirmed that positively charged pollutants such as amitriptyline and

verapamil showed good adsorption to MX.[104] The kinetics of adsorption were studied using two different sonication frequencies (28 and 570 kHz). Low frequency sonication improved the degradation performance by producing larger cavitations when compared to the high frequency ultrasound. Due to the unique surface morphological properties of MXene,

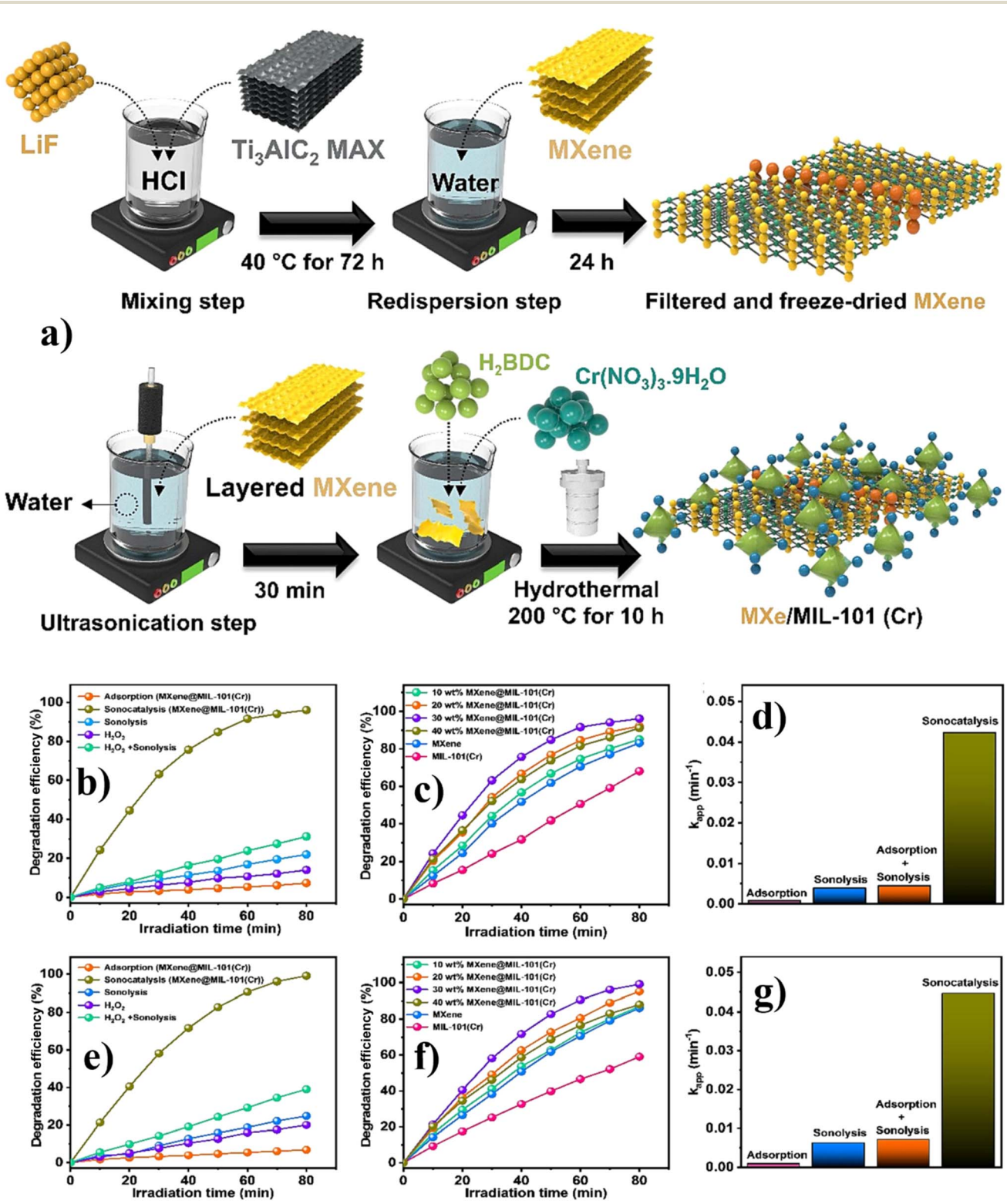

Fig. 14 (a) Schematic representation of MX@MIL-101 (Cr) preparation (b & e) degradation efficiency of various AOPs with radical promoters against sulfadiazine and acetaminophen (c & f) Effect of MXene loading on degradation efficiency against sulfadiazine and acetaminophen (d & g) representative bar graphs illustrating the synergistic effect of the sonocatalytic process.

numerous combinations have been reported to date (Table 1). However, MXene-based nanocatalysts for environmental applications have predominantly focused on metal oxide-derived MXene composites. While Metal Organic Framework (MOF)-based nanocatalysts have gained significant attention in recent years, the potential of MXene/MOF-based nanocatalysts for environmental applications remains relatively unexplored compared to their metal oxide counterparts. S. Ranjith *et al.* prepared an MOF-supported MXene-based sonocatalyst for the elimination of sulfadiazine (SD) and acetaminophen (AAP) in aquatic conditions.[105] The MXene was synthesized *via* chemical etching of the MAX phase and MX@MOF combination were prepared using H_2BDC and Cr salt along with the layered MXene under a hydrothermal route, as illustrated in Fig. 14a. The concentrations of the synthesized MX@MIL-101 were optimized and employed to degrade SD and AAP under various AOPs (Fig. 14b, c, e, and f). The MX@MIL-101 nanocatalyst demonstrated promising removal efficiencies of up to ~96% for SD and ~99% for AAP, indicating that MXene is highly suitable for heterogeneous nucleation and for reducing recombination with MOF derived nanostructures, as shown in Fig. 14d and g. Yang *et al.* synthesized MIL-125 (Ti) supported with $Ti_3C_2T_x$ MXene using hydrothermal treatment and investigated its efficacy in degrading Rhodamine B (RhB) and microplastics (MP) under sonocatalytic conditions.[130] The synthesized MX@MOF nanocatalyst demonstrated the ability to degrade RhB up to 93.1% and decompose MP up to 78% without the use of any radical promoters. Optimization of catalyst dosage and ultrasonic (US) power was conducted to enhance the degradation efficiency. The authors described MXene as an electron trap, where the sonoluminescence-excited electrons of MIL-125 can migrate to the MXene band, thereby reducing the recombination effect.

Unlike sonocatalysis or sonophotocatalysis, the exploration of MXene in photocatalysis is more extensive and well-developed. Various combinations of nanocatalysts have been employed with MXene for multifaceted applications.[106–108] In the context of photocatalytic wastewater treatment, notable work was initiated by Chao Peng *et al.*, synthesized $Ti_3C_2T_x$-supported TiO_2 nanocatalyst for the removal of Methyl Orange under photocatalytic conditions.[109] The authors described MXene as forming a "Schottky junction with 2D Ti_3C_2 acting as a reservoir of holes". Since this work was reported in 2016, research on MXene-based photocatalysis has grown exponentially. Numerous contaminants and catalyst combinations have been proposed; however, addressing all of them is beyond the scope of this review and many review have been already established in terms of photocatalysis and MXene.[110–113] Therefore, we have summarized selected works that align with our current review's objectives, focusing on value addition by heterojunctions.

4.5 Limitations and trade-offs of MXene based nanoarchitectures

Evaluation of compromising trade-offs is essential to translating MXene-based nanoarchitectures to real-world wastewater applications such as h-AOP technologies. Upon careful analysis on various MXene-based nanocomposites for organic contaminants degradation, several limitations from the materials side were observed in related to sonocatalysis, photocatalysis and sonophotocatalysis. The major limitations and trade-offs of MXene are; (1) prone to surface oxidation of Ti_3C_2 to metal oxides (2) structural stability of MXene layers under strong acidic or basic conditions (3) hydrophobicity of M–X layers that limit the scope of contaminants (4) scalability and reproducibility of highly surface engineered MXenes (5) lack of regulatory terms for environmental and biological impacts of MXenes. In context to the trade-offs, Lukatskaya *et al.* demonstrated the potential of MXenes for energy storage applications, highlighting the high volumetric capacitance of Ti_3C_2 MXene enabled by reversible cation intercalation. However, their study also revealed a key limitation: MXenes are prone to oxidation in aqueous environments, which can degrade their conductivity and long-term performance.[114] Additionally, the hydrophobic nature of MXene surfaces can lead to pH-dependent surface charge variations which may restrict the electrostatic attraction and adsorption of a broad range of organic contaminants in water.[81] Under sonocatalytic conditions, although MXenes can promote heterogeneous nucleation of cavitation bubbles, the intense US energy can lead to partial surface oxidation, forming TiO_2, which alters the material's original catalytic characteristics.[98] Indeed, the use of MXenes in nanocomposites typically involves low concentrations and recent advancements in near eco-friendly synthesis methods suggest that these trade-offs may be addressed through future process intensification studies.

5. Synergy effect of h-AOP processes

The sonophotocatalytic processes provide a better platform for the degradation of toxic contaminants through six combined processes (sonolysis, photolysis, photocatalysis, sonocatalysis, sonophotolysis and sonophotocatalysis),[31] compared to the sono and photo-alone processes. The combination of six processes at once would result in increased efficiency and enhanced mineralization. The enhancement is considered to be an outcome of the synergistic effects of sono and photocatalysis as discussed in 2.2. Various researchers investigated about the synergistic effect of their catalysts' performances in sonophotocatalysis. The synergistic effect of the sonophotocatalytic study can be evaluated by the rate constants obtained from the individual degradation study such as sonocatalysis and photocatalysis along with sonophotocatalysis. The precise method to assess the synergistic effect of sonophotocatalysis is to find the synergy index or percentage of synergism. The eqn (3) is the synergy index formula for the evaluation of synergy effect resulted from the h-AOPs.

$$\text{Synergy index} = \frac{k_{\text{sonophotocatalysis}}}{k_{\text{sonocatalysis}} + k_{\text{photocatalysis}}} \quad (3)$$

$$\text{Percentage of synergy} = \frac{k_{\text{sonophotocatalysis}} - \left(k_{\text{sonocatalysis}} + k_{\text{photocatalysis}}\right)}{k_{\text{sonophotocatalysis}}} \times 100 \quad (4)$$

$$\text{True synergy index} = \frac{k_{\text{sonophotocatalysis}} - \left(k_{\text{sonolysis}} + k_{\text{photolysis}} + k_{\text{sonocatalysis}} + k_{\text{photocatalysis}}\right)}{k_{\text{sonophotocatalysis}}} \quad (5)$$

whereas $k_{\text{sonocatalysis}}$, $k_{\text{photocatalysis}}$, and $k_{\text{sonophotocatalysis}}$ are the rate constants of sonocatalysis, photocatalysis and sonophotocatalysis, respectively. The evaluation of synergy index varies based on the involvement of the distinct processes. In addition, synergy index and % are expressed mathematically in eqn (3) and (4), respectively. Using eqn (3), the corresponding value demonstrates the involvement of sonophotolysis and sonophotocatalysis. However, to examine the true synergy of h-AOP processes, eqn (5) must be taken into account in which the rate constants of sonolysis and photolysis are also adopted. The synergy index is completely dependent on the type of degradation system (light source, power, frequency). Nonetheless, various synergy index expression has also been proposed over the years, some of them are represented in the following eqn (6) and (7).[115]

$$\text{Synergy index of SR mediated hybrid} - \text{AOP} = \frac{k_{\text{sonophotocatalysis}} + \text{PMS}}{k_{\text{sonocatalysis}} + \text{PMS} + k_{\text{photocatalysis}} + \text{PMS}} \quad (6)$$

$$\text{Synergy index of hybrid AOP with addition of } H_2O_2 = \frac{k_{\text{sonophotocatalysis}} + H_2O_2}{k_{\text{sonocatalysis}} + H_2O_2 + k_{\text{photocatalysis}} + H_2O_2} \quad (7)$$

Various reports were discussed about the synergism in sonophotocatalytic processes and other h-AOPs.[115–121] For instance, K. Yun *et al.* evaluated the synergistic effect of ultrasound irradiation and light energy in the sonophotocatalytic degradation of ciprofloxacin. A synergy up to 68% between ultrasound and light was achieved, based on the comparison of single handed AOPs.[122] While some studies report synergy as a percentage to indicate the enhancement, the use of a synergy index (S. I.) is a more appropriate and standardized approach. Typically, the S. I. value may be greater than, equal to, or less than unity, for synergistic, additive, or antagonistic effects, respectively. The effective surface cleaning of nanocatalysts by US and the enhanced light penetration due to US-induced turbulence can complement each other during the degradation process resulting in a S. I. greater than unity. In most cases, the S. I. values for sonophotocatalytic systems range between 0.7 to 2.0. This variation is attributed to several factors influencing the h-AOP, including the efficient properties of the nanocatalyst, the wavelength of the light source, nature of the contaminant, and frequency/power of US irradiation. An S. I. value less than one may indicate limitations such as poor light penetration, shielding or scattering effects, mismatched US energy, catalyst deactivation, or even catalyst leaching. Notably few studies on sonophotocatalytic degradation of organic pollutants have evaluated the synergy index using eqn (4).[123,124] However, the reports of MXene in sonophotocatalytic environmental remediation is still limited and requires more extensive studies in the future. Additionally, we observed that the existing reports on MXene in sonophotocatalysis have not adequately addressed the evaluation of synergistic effects. Therefore, future studies should incorporate such evaluations to enhance the understanding of h-AOPs.

6. Perspectives of the research in future

6.1 Degradation pathway

Although significant advancements have been made in the hazardous pollutant degradation using AOP technologies like sonocatalysis or photocatalysis, a major gap remains in understanding the precise degradation mechanisms and pathways. Future studies should prioritize: quantitative identification of reactive species generated during the degradation processes, Toxicological evaluation of intermediate compounds formed during reactions, and mechanistic analysis to determine the individual and hybrid contributions of photo- and ultrasonic-effects to ROS formation and pollutant breakdown. These aspects are often overlooked or not presented alongside degradation results, yet limiting the assessment of secondary pollution risks. Developing standardized protocols for degradation pathway analysis and integrating them into routine evaluations will enable a more comprehensive and environmentally responsible application of h-AOPs in wastewater treatment. Furthermore, extensive studies on the degradation pathway and intermediate analysis should be the primary focus of future research in this area.

6.2 Multiple pollutants removal

Many studies have concentrated on eliminating a single contaminant class. In real-time scenario, wastewater effluents may contain multiple contaminants.[133] In light of this, multiple pollutant removal must be investigated in order to mimic natural system, commercialise the process and advance the practical applications. Future research should address: synergistic or antagonistic interactions between different classes of organic contaminants, efficacy of AOPs in mixed pollutant systems, and design of hybrid or modular AOP systems that can adaptively eliminate a range of co-existing pollutants. Such direction of investigations are essential to move from laboratory-scale models toward commercial viability and real-world deployment of AOP technologies.

6.3 Operational conditions and advanced materials

Despite diverse reports on sonocatalytic, photocatalytic, and sonophotocatalytic degradation using various instruments

and conditions, there remain a need for: systematic comparisons of operation modes such as simultaneous, sequential, and interval based treatment conditions to better understand their effects on degradation efficiency and energy consumption, development of frequency varied sonication probes and multi-frequency ultrasound systems to enhance efficiency intensification and higher reactivity and emphasis on eco-friendly/non-toxic catalyst materials capable of large-scale usage without generating harmful residues. Special attention should be given to green-synthesized MXenes in these applications which could provide valuable insights and direct future research efforts.

Table 2 Overview of merits and demerits in various MXene synthesis techniques

S. no.	Synthesis methodology	Merits	Demerits	Ref.
1	HF etching (direct etching)	• Simple and straightforward • Widely used • High yield of MXene nanosheets	• Hazardous HF handling • Environment and safety concerns	160
2	*In situ* HF etching (*e.g.*, LiF + HCl)	• Safer than direct HF • Tunable surface terminations	• Longer reaction time • Incomplete etching of MAX phases	161
3	Molten salt etching	• HF-free • Potential for large scale and clean synthesis	• Requires high temperature • Could alter resulting MXene composition	162
4	Electrochemical etching	• Cleaner method • Controllable reaction conditions • HF-free	• Toxicity depends on electrolyte; some may be corrosive or hazardous • Limited to conductive MAX phases	163
5	Alkali-assisted etching	• Safer than HF method • It can introduce oxygen functional groups	• Low etching efficiency • Stronger concentration required • Structural degradation possible	164
6	Hydrothermal etching	• Possible HF-free approach • Enables tunable surface terminations • Suitable eco-friendly specific functionalization	• Often requires high temperature and longer reaction time • Safety still depends on etchant used	165
7	Sonochemical etching	• Rapid exfoliation • Prevents restacking of layers • Aids surface activation and cleaning	• Not a standalone etching methodology • Safety depends on chemicals used	166
8	Organic salts assisted etching	• Safer alternative to HF etching • Enables various surface terminations	• Reagent cost may be higher • Safety and eco-friendliness still depend on the etchant used	167
9	Halogen etching	• HF-free approach • Can be done in room or low temperature conditions • Enables surface termination control • Avoids harsh acid/base treatments	• Involves toxic and volatile halogens • Requires inert atmosphere and anhydrous solvents • Need cryogenic or heated conditions • Scalability limited	168

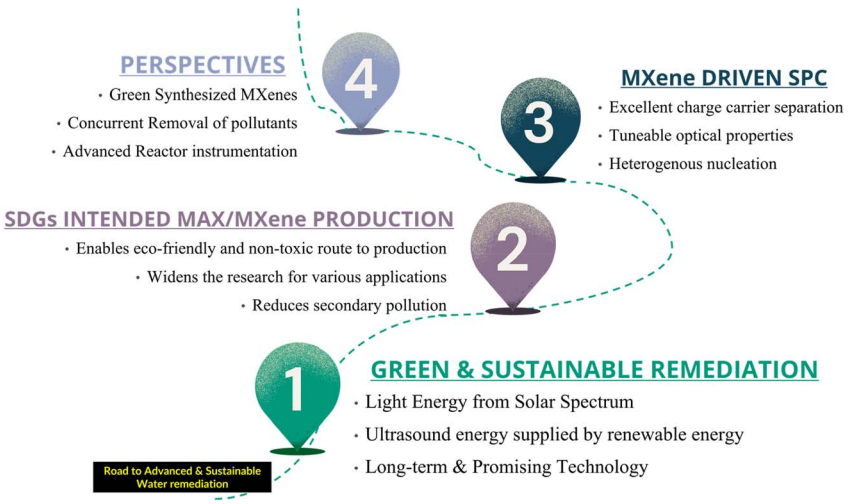

Fig. 15 Schematic roadmap summarizing the key themes and future directions discussed in this review.

7. Conclusion

The current wastewater treatment technologies often fail to reduce secondary pollution and are inefficient in terms of catalytic conversion, especially in the current population growth and industrialization. The 6th and 12th SDGs call for the development of sustainable technologies and materials to eliminate toxic contaminants from water environments. Recent studies highlight the positive synergy effect of sonophotocatalysis, addressing many of the practical limitations associated with traditional methods. These studies demonstrate that sonophotocatalysis can reduce treatment times and achieve more effective degradation, owing to the cooperative interaction between sonocatalysis and photocatalysis. On the materials side, the rise of MXene-based nanocatalysts for the degradation of various environmental pollutants presents promising alternatives for water remediation. The growing attention towards MXene synthesis in green and environmentally safer routes were summarised with their prospects and future directions (Table 2). The potential industrial-scale synthesis routes for MXene and its precursors (MAX) in catalyst production have been critically examined in relation to SDG targets. Moreover, the flexibility of MXene-assisted sonophotocatalysis has been thoroughly explored, and the available findings have been summarized in a comprehensive table to guide future research. The functional properties of MXene in relation to catalytic activation under visible-light irradiation and US energy have been comprehensively discussed. However, the simultaneous removal of multiple pollutants using sono, photo, and sonophotocatalytic processes, along with a deeper analysis of the synergistic effects, remains an area that requires further attention. Future studies should also focus on investigating advanced intermediates, quantifying ROS, and exploring the commercialization potential of MXene-based h-AOPs. The overall summary of this review is presented in Fig. 15. These aspects will be crucial in advancing the field and realizing the full potential of MXene in wastewater remediation applications, particularly in AOPs.

Conflicts of interest

The authors declare that they have no known competing financial interests or personal relationships that could appear to influence the work reported in this paper.

Data availability

No primary research results, software or code have been included and no new data were generated or analyzed as part of this review.

Acknowledgements

The authors thank VIT for providing 'VIT SEED GRANT (RGEMS) – Sanctioned Order No. SG20230012' for carrying out this research work.

References

1 Progress on Ambient Water Quality – 2024 Update, 2024.
2 S. N. Malik, *et al.*, Hybrid ozonation process for industrial wastewater treatment: Principles and applications: A review, *J. Water Process Eng.*, 2020, **35**, 101193.
3 J. Zeng, *et al.*, Quenching residual H2O2 from UV/H2O2 with granular activated carbon: A significant impact of bicarbonate, *Chemosphere*, 2024, **354**, 141670.
4 S. Lim, *et al.*, Ozonation of organic compounds in water and wastewater: A critical review, *Water Res.*, 2022, **213**, 118053.
5 K. Obaideen, *et al.*, The role of wastewater treatment in achieving sustainable development goals (SDGs) and sustainability guideline, *Energy Nexus*, 2022, **7**, 100112.
6 A. Gulzar, *et al.*, Harnessing the power of MXenes: a comprehensive exploration of their photocatalytic potential in mitigating hazardous dyes and CO2 reduction, *Discover Mater.*, 2024, **4**(1), 15.
7 K. Fedorov, *et al.*, Synergistic effects of hybrid advanced oxidation processes (AOPs) based on hydrodynamic cavitation phenomenon – A review, *Chem. Eng. J.*, 2022, **432**, 134191.
8 M. Pirsaheb and N. Moradi, A systematic review of the sonophotocatalytic process for the decolorization of dyes in aqueous solution: Synergistic mechanisms, degradation pathways, and process optimization, *J. Water Process Eng.*, 2021, **44**, 102314.
9 C. Ashina, *et al.*, Review on enhancing solar photocatalysis for sustainable degradation of invisible environmental pollutants, *Renewable Sustainable Energy Rev.*, 2025, **214**, 115490.
10 S. K. Sheik Moideen Thaha, *et al.*, Low-frequency ultrasound-enabled synthesis of Ag/TiO_2/g-C_3N_4 nanocomposites for efficient visible-light-driven photocatalysis, *Mater. Sci. Eng., B*, 2025, **320**, 118408.
11 M. L. Puga, *et al.*, Aluminium-doped TiO2 nanotubes with enhanced light-harvesting properties, *Ceram. Int.*, 2021, **47**(13), 18358–18366.
12 P. Sathishkumar, *et al.*, Synthesis of CuO-ZnO nanophotocatalyst for visible light assisted degradation of a textile dye in aqueous solution, *Chem. Eng. J.*, 2011, **171**(1), 136–140.
13 C. L. Brito, *et al.*, A Review on Carbon Nanotubes Family of Nanomaterials and Their Health Field, *ACS Omega*, 2024, **9**(8), 8687–8708.
14 Y. Luo, D. He and G. Qing, Investigation into the Impact of Fe2O3, MgO, and Al2O3 Contents on the Ca Ions Leaching Rate of Steel Slag, *JOM*, 2024, **76**(3), 1356–1371.
15 S. Thakur, *et al.*, Advances in powder nano-photocatalysts as pollutant removal and as emerging contaminants in water: Analysis of pros and cons on health and environment, *Adv. Powder Mater.*, 2024, **3**(6), 100233.
16 A. Hoseini and B. Yarmand, Enhanced photocatalytic performance and photocorrosion stability of PEO-immobilized TiO2 photocatalyst using rGO/Fe2O3 sensitizers, *Surf. Interfaces*, 2023, **42**, 103424.

17 M. Dimitropoulos, *et al.*, Unveiling the photocorrosion mechanism of zinc oxide photocatalyst: Interplay between surface corrosion and regeneration, *J. Environ. Chem. Eng.*, 2024, **12**(2), 112102.
18 L. Liang and X. Shi, Electrochemical and photocatalytic properties of ZnO nanostructures deposited on nanoporous anodized aluminum oxide membrane and its application for degradation of reactive blue 19 in textile wastewater, *Int. J. Electrochem. Sci.*, 2023, **18**(9), 100272.
19 H. Dong, *et al.*, An overview on limitations of TiO2-based particles for photocatalytic degradation of organic pollutants and the corresponding countermeasures, *Water Res.*, 2015, **79**, 128–146.
20 S. A. Ahire, *et al.*, The Augmentation of nanotechnology era: A concise review on fundamental concepts of nanotechnology and applications in material science and technology, *Results Chem.*, 2022, **4**, 100633.
21 B. R. Anne, *et al.*, A Review on MXene as Promising Support Materials for Oxygen Evolution Reaction Catalysts, *Adv. Funct. Mater.*, 2023, **33**(51), 2306100.
22 B. Miao, *et al.*, Impact of various 2D MXene surface terminating groups in energy conversion, *Renewable Sustainable Energy Rev.*, 2024, **199**, 114506.
23 T. Bashir, *et al.*, MXene terminating groups O, –F or –OH, –F or O, –OH, –F, or O, –OH, –Cl?, *J. Energy Chem.*, 2023, **76**, 90–104.
24 M. Naguib, *et al.*, Two-Dimensional Nanocrystals Produced by Exfoliation of Ti3AlC2, *Adv. Mater.*, 2011, **23**(37), 4248–4253.
25 Y. Vasseghian, *et al.*, A comprehensive review on MXenes as new nanomaterials for degradation of hazardous pollutants: Deployment as heterogeneous sonocatalysis, *Chemosphere*, 2022, **287**, 132387.
26 M. Mohammadi, *et al.*, Chapter 10 - MXenes for removal of pharmaceutical-based pollutants, in *Mxene-Based Hybrid Nano-Architectures for Environmental Remediation and Sensor Applications*, ed. R. K. Gupta, et al., Elsevier, 2024, pp. 199–217.
27 J. K. Im, *et al.*, Review of MXene-based nanocomposites for photocatalysis, *Chemosphere*, 2021, **270**, 129478.
28 B. Bhattacharjee, *et al.*, Advances in 2D MXenes-based materials for water purification and disinfection: Synthesis approaches and photocatalytic mechanistic pathways, *J. Environ. Manage.*, 2022, **324**, 116387.
29 X. Xu, *et al.*, Study on ultrasonic treatment for municipal sludge, *Ultrason. Sonochem.*, 2019, **57**, 29–37.
30 S. Pilli, *et al.*, Ultrasonic pretreatment of sludge: A review, *Ultrason. Sonochem.*, 2011, **18**(1), 1–18.
31 P. Sathishkumar, R. V. Mangalaraja and S. Anandan, Review on the recent improvements in sonochemical and combined sonochemical oxidation processes – A powerful tool for destruction of environmental contaminants, *Renewable Sustainable Energy Rev.*, 2016, **55**, 426–454.
32 W. Li, *et al.*, Photocatalysis of Clofibric Acid under Solar Light in Summer and Winter Seasons, *Ind. Eng. Chem. Res.*, 2011, **50**(9), 5384–5393.
33 J. Gomes, *et al.*, Advanced oxidation processes for recalcitrant compounds removal comparison with biofiltration by Corbicula fluminea, *Energy Rep.*, 2020, **6**, 666–671.
34 E. Kuna, *et al.*, Sonocatalysis: A Potential Sustainable Pathway for the Valorization of Lignocellulosic Biomass and Derivatives, *Top. Curr. Chem.*, 2017, **375**(2), 41.
35 S. K. S. M. Thaha, *et al.*, Critical Review of Photocatalytic Reactor Designs for Environmental Applications, in *Photocatalysis for Energy and Environmental Applications: Current Trends and Future Perspectives*, ed. P. Sathishkumar, Springer Nature Singapore, Singapore, 2024, pp. 1–50.
36 M. H. Abdurahman, A. Z. Abdullah and N. F. Shoparwe, A comprehensive review on sonocatalytic, photocatalytic, and sonophotocatalytic processes for the degradation of antibiotics in water: Synergistic mechanism and degradation pathway, *Chem. Eng. J.*, 2021, **413**, 127412.
37 T. Leong, M. Ashokkumar and S. Kentish, The Fundamentals of Power Ultrasound – A Review, *Acoustics Australia*, 2011, **39**(2), 54–63.
38 R. Pflieger, *et al.*, Sonoluminescence, in *Characterization of Cavitation Bubbles and Sonoluminescence*, 2019, pp. 39–60.
39 M. A. Beckett and I. Hua, Impact of Ultrasonic Frequency on Aqueous Sonoluminescence and Sonochemistry, *J. Phys. Chem. A*, 2001, **105**(15), 3796–3802.
40 P. Qiu, *et al.*, A review on heterogeneous sonocatalyst for treatment of organic pollutants in aqueous phase based on catalytic mechanism, *Ultrason. Sonochem.*, 2018, **45**, 29–49.
41 G. Wang and H. Cheng, Application of Photocatalysis and Sonocatalysis for Treatment of Organic Dye Wastewater and the Synergistic Effect of Ultrasound and Light, *Molecules*, 2023, **28**(9), 3706.
42 K. S. Suslick, Sonochemistry, *Science*, 1990, **247**(4949), 1439–1445.
43 M. Sun, *et al.*, Thermally-assisted photocatalytic CO2 reduction to fuels, *Chem. Eng. J.*, 2021, **408**, 127280.
44 H. Wang, *et al.*, Solar-heating boosted catalytic reduction of CO2 under full-solar spectrum, *Chin. J. Catal.*, 2020, **41**(1), 131–139.
45 R. Acharya and K. Parida, A review on TiO2/g-C3N4 visible-light- responsive photocatalysts for sustainable energy generation and environmental remediation, *J. Environ. Chem. Eng.*, 2020, **8**(4), 103896.
46 R. Acharya, L. Acharya, and K. Parida, BiFeO 3 -Based Materials For Augmented Photoactivity, in *Perovskite Materials for Energy and Environmental Applications*, 2022, pp. 167–216.
47 J. Madhavan, *et al.*, Degradation of acid red 88 by the combination of sonolysis and photocatalysis, *Sep. Purif. Technol.*, 2010, **74**(3), 336–341.
48 C. G. Joseph, *et al.*, Operating parameters and synergistic effects of combining ultrasound and ultraviolet irradiation in the degradation of 2,4,6-trichlorophenol, *Desalination*, 2011, **276**(1), 303–309.

49 J. Madhavan, *et al.*, Ultrasound assisted photocatalytic degradation of diclofenac in an aqueous environment, *Chemosphere*, 2010, **80**(7), 747–752.
50 S. Chakma and V. S. Moholkar, Investigation in mechanistic issues of sonocatalysis and sonophotocatalysis using pure and doped photocatalysts, *Ultrason. Sonochem.*, 2015, **22**, 287–299.
51 K. Dennerlein, *et al.*, Dermal absorption and skin damage following hydrofluoric acid exposure in an ex vivo human skin model, *Toxicol. Lett.*, 2016, **248**, 25–33.
52 T. Cernev and R. Fenner, The importance of achieving foundational Sustainable Development Goals in reducing global risk, *Futures*, 2020, **115**, 102492.
53 J. Serafin, *et al.*, Comprehensive analysis of MAX phase and MXene materials for advanced photocatalysis, electrocatalysis and adsorption in hydrogen evolution and storage, *J. Ind. Eng. Chem.*, 2025, **142**, 18–33.
54 M. Downes, *et al.*, Comprehensive synthesis of Ti3C2Tx from MAX phase to MXene, *Nat. Protoc.*, 2024, **19**(6), 1807–1834.
55 J. Li, L. Yang and H. Long, Climatic impacts on energy consumption: Intensive and extensive margins, *Energy Econ.*, 2018, **71**, 332–343.
56 V. L. Trinh and C. K. Chung, Renewable energy for SDG-7 and sustainable electrical production, integration, industrial application, and globalization: Review, *Cleaner Eng. Technol.*, 2023, **15**, 100657.
57 T. Yang, *et al.*, Low-temperature synthesis of Ti3Al(Sn)C2 solid solution using replacement reaction, *J. Mater. Sci.: Mater. Electron.*, 2020, **31**(22), 20601–20610.
58 Z. Li, *et al.*, HiPIMS induced high-purity Ti3AlC2 MAX phase coating at low-temperature of 700 °C, *J. Eur. Ceram. Soc.*, 2023, **43**(11), 4673–4683.
59 J. Sinclair, *et al.*, Sol Gel-Based Synthesis of the Phosphorus-Containing MAX Phase V2PC, *Inorg. Chem.*, 2022, **61**(43), 16976–16980.
60 J. P. Siebert, M. Flores and C. S. Birkel, Shape Control of MAX Phases by Biopolymer Sol–Gel Synthesis: Cr2GaC Thick Films, Microspheres, and Hollow Microspheres, *ACS Org. Inorg. Au*, 2022, **2**(1), 59–65.
61 J. P. Siebert, *et al.*, Sol–gel based synthesis and enhanced processability of MAX phase Cr2GaC, *J. Mater. Chem. C*, 2019, **7**(20), 6034–6040.
62 R. Torres-Sánchez, *et al.*, Hydrogen fluoride concentrations in ambient air of an urban area based on the emissions of a major phosphogypsum deposit (SW, Europe), *Sci. Total Environ.*, 2020, **714**, 136891.
63 Y. Zhang, *et al.*, Injuries following a serious hydrofluoric acid leak: First aid and lessons, *Burns*, 2015, **41**(7), 1593–1598.
64 T. F. Li, *et al.*, Fluorine-Free Synthesis of High-Purity Ti3C2Tx (T = OH, O) via Alkali Treatment, *Angew. Chem., Int. Ed.*, 2018, **57**, 6115.
65 S. Saxena, *et al.*, Thinking green with 2-D and 3-D MXenes: Environment friendly synthesis and industrial scale applications and global impact, *Renewable Sustainable Energy Rev.*, 2023, **178**, 113238.
66 S. Bilge and A. Sınağ, Current trends and strategies in the development of green MXene-based photoelectrochemical sensing application, *TrAC, Trends Anal. Chem.*, 2023, **163**, 117059.
67 J. Zhu, *et al.*, Solvent-free one-step green synthesis of MXenes by "gas-phase selective etching, *Energy Storage Mater.*, 2024, **70**, 103503.
68 P. A. Rasheed, *et al.*, Ecotoxicity and environmental safety assessment of two-dimensional niobium carbides (MXenes), *Sci. Total Environ.*, 2024, **947**, 174563.
69 I. A. Vasyukova, *et al.*, Synthesis, Toxicity Assessment, Environmental and Biomedical Applications of MXenes: A Review, *Nanomaterials*, 2022, **12**(11), 1797.
70 R. P. Pandey, *et al.*, Effect of Sheet Size and Atomic Structure on the Antibacterial Activity of Nb-MXene Nanosheets, *ACS Appl. Nano Mater.*, 2020, **3**(11), 11372–11382.
71 S. F. Hansen, *et al.*, Maximizing the safety and sustainability of MXenes, *Sci. Rep.*, 2024, **14**(1), 31030.
72 W. Wu, *et al.*, Evaluating the Cytotoxicity of Ti3C2 MXene to Neural Stem Cells, *Chem. Res. Toxicol.*, 2020, **33**(12), 2953–2962.
73 G. K. Nasrallah, *et al.*, Ecotoxicological assessment of Ti3C2Tx (MXene) using a zebrafish embryo model, *Environ. Sci.: Nano*, 2018, **5**(4), 1002–1011.
74 J. Wu, Y. Yu and G. Su, Safety Assessment of 2D MXenes: In Vitro and In Vivo, *Nanomaterials*, 2022, **12**(5), 828.
75 J. Chen, *et al.*, Recent progress and advances in the environmental applications of MXene related materials, *Nanoscale*, 2020, **12**(6), 3574–3592.
76 M. Ikram, *et al.*, A review of photocatalytic characterization, and environmental cleaning, of metal oxide nanostructured materials, *Sustainable Mater.Technol.*, 2021, **30**, e00343.
77 Z. Wang, *et al.*, Recent progress of MXene as a cocatalyst in photocatalytic carbon dioxide reduction, *Chem. Eng. J. Adv.*, 2024, **18**, 100593.
78 Y. Kumar, *et al.*, Exploring MXenes and MAX phases: Advancements in properties, synthesis, and application, *Inorg. Chem. Commun.*, 2024, **170**, 113531.
79 B. J. Janani, *et al.*, Robust advantage of MXene/g-C3N4 loaded on Fe2WO6/BiIO4 nano-platform for chemo-peroxidase colorimetric detection of uranyl ions, antifungal properties, photocatalytic degradation of p-chlorophenol, and eco-toxicity studies, *Diamond Relat. Mater.*, 2024, **145**, 111129.
80 D. Anand Upar, *et al.*, Exfoliated g-C3N4-CdS-MXene an efficient all-solid-state Z-type heterojunction serving as efficient photo/electro/photoeletro catalyst for oxygen evolution reaction and dye degradation under visible light at low bias voltage, *Appl. Surf. Sci.*, 2024, **677**, 161030.
81 B. M. Jun, *et al.*, Ultrasonic degradation of selected dyes using Ti(3)C(2)T(x) MXene as a sonocatalyst, *Ultrason. Sonochem.*, 2020, **64**, 104993.
82 S. Wang, *et al.*, Identifying the surface properties of Ti3C2Tx MXene through transmission electron microscopy, *Cell Rep. Phys. Sci.*, 2022, **3**(11), 101151.
83 K. Yasui, Fundamentals of Acoustic Cavitation and Sonochemistry, in *Theoretical and Experimental*

Sonochemistry Involving Inorganic Systems, ed. M. Ashokkumar, Springer Netherlands, Dordrecht, 2011, pp. 1–29.

84 S. Mishra, *et al.*, Boosted photocatalytic accomplishment of 3D/2D hierarchical structured Bi4O5I2/g-C3N4 p–n type direct Z-scheme heterojunction towards synchronous elimination of Cr(VI) and tetracycline, *Diamond Relat. Mater.*, 2024, **142**, 110834.

85 S. Mishra, *et al.*, Graphitic carbon nitride loaded Bi4O5I2 for elevated photocatalytic tetracycline degradation, *J. Met. Mater. Miner.*, 2025, **35**(2), e2261.

86 K. Gao, *et al.*, BiOBr/MXene/gC3N4 Z-scheme heterostructure photocatalysts mediated by oxygen vacancies and MXene quantum dots for tetracycline degradation: Process, mechanism and toxicity analysis, *Appl. Catal., B*, 2023, **323**, 122150.

87 S. Li, *et al.*, A novel MXene-bridged Z-scheme ZnO@Nb2CTx MXene@carbon nitride nanosheets photocatalyst for efficient enrofloxacin degradation, *Chem. Eng. J.*, 2024, **489**, 151505.

88 P. Kumari, *et al.*, Engineering Schottky-like and heterojunction materials for enhanced photocatalysis performance – a review, *Mater. Adv.*, 2022, **3**(5), 2309–2323.

89 S. Mishra and R. Acharya, Recent updates in modification strategies for escalated performance of Graphene/MFe2O4 heterostructured photocatalysts towards energy and environmental applications, *J. Alloys Compd.*, 2023, **960**, 170576.

90 R. Acharya, S. Pati and K. Parida, A review on visible light driven spinel ferrite-g-C3N4 photocatalytic systems with enhanced solar light utilization, *J. Mol. Liq.*, 2022, **357**, 119105.

91 D.-E. Lee, *et al.*, A hierarchical 3D hybrid CoAl-layered double hydroxide/TiO2/Ti3C2 MXene S-scheme photocatalyst with 2D/0D/2D contact interfaces for sustainable pollutant degradation, *Appl. Surf. Sci.*, 2024, **649**, 159178.

92 C. Yao, *et al.*, 2D/2D α-Fe2O3/single-layer MXene Schottky photocatalysis-PMS activation bidirectionally enhanced coupling system for environmental remediation, *J. Alloys Compd.*, 2023, **941**, 168920.

93 K. Liu, *et al.*, Oxygen-functionalized Ti3C2 MXene/exfoliated montmorillonite supported S-scheme BiOBr/Bi2MoO6 heterostructures for efficient photocatalytic quinolone antibiotics degradation, *Chem. Eng. J.*, 2023, **457**, 141271.

94 Y. Wu, *et al.*, In-situ annealed "M-scheme" MXene-based photocatalyst for enhanced photoelectric performance and highly selective CO2 photoreduction, *Nano Energy*, 2021, **90**, 106532.

95 Z. Yao, *et al.*, 2D/2D Heterojunction of R-scheme Ti3C2 MXene/MoS2 Nanosheets for Enhanced Photocatalytic Performance, *Nanoscale Res. Lett.*, 2020, **15**(1), 78.

96 C. Cui, *et al.*, Bi2WO6/Nb2CTx MXene hybrid nanosheets with enhanced visible-light-driven photocatalytic activity for organic pollutants degradation, *Appl. Surf. Sci.*, 2020, **505**, 144595.

97 Y. Zhang, *et al.*, Ti3C2T MXene supported ZnO nanocomposites with highly efficient photocatalytic performance for degradation of VOCs, *Diamond Relat. Mater.*, 2023, **133**, 109763.

98 K. S. Ranjith, *et al.*, WS2-intercalated Ti3C2Tx MXene/TiO2-stacked hybrid structure as an excellent sonophotocatalyst for tetracycline degradation and nitrogen fixation, *Ultrason. Sonochem.*, 2023, **100**, 106623.

99 S. K. Sheik Moideen Thaha and P. Sathishkumar, Bisphenol A/Bisphenol F mineralization in the presence of self-decorated carbon-QDs@Bi2O2CO3/Ti3C2/g-C3N4 nanocomposites under multi-frequency ultrasound assisted sonophotocatalysis, *Chem. Eng. J.*, 2025, **505**, 159578.

100 Q. Li, *et al.*, Schottky heterojunction-based photocatalysis-in-situ-self-Fenton system: Removal of tetracycline hydrochloride and biotoxicity evaluation of intermediates, *Appl. Catal., B*, 2025, **360**, 124533.

101 S. Birudukota, *et al.*, Risk-based in silico mutagenic assessment of benzodiazepine impurities using three QSAR tools, *Toxicol Rep*, 2025, **14**, 102008.

102 S. Kim, *et al.*, Effect of single and multilayered Ti(3)C(2)T(X) MXene as a catalyst and adsorbent on enhanced sonodegradation of diclofenac and verapamil, *J. Hazard. Mater.*, 2022, **426**, 128120.

103 P. Sathishkumar, *et al.*, Contemporary Achievements of Visible Light-Driven Nanocatalysts for the Environmental Applications, in *Photocatalytic Functional Materials for Environmental Remediation*, 2019, pp. 69–129.

104 S. Kim, *et al.*, Enhanced adsorption performance for selected pharmaceutical compounds by sonicated Ti3C2TX MXene, *Chem. Eng. J.*, 2021, 406.

105 K. Shanmugam Ranjith, *et al.*, Synergistic effects of layered Ti3C2TX MXene/MIL-101(Cr) heterostructure as a sonocatalyst for efficient degradation of sulfadiazine and acetaminophen in water, *Ultrason. Sonochem.*, 2023, **99**, 106570.

106 B. Anasori, M. R. Lukatskaya and Y. Gogotsi, 2D metal carbides and nitrides (MXenes) for energy storage, *Nat. Rev. Mater.*, 2017, **2**, 16098.

107 S. M. Majhi, *et al.*, V2CTX MXene-based hybrid sensor with high selectivity and ppb-level detection for acetone at room temperature, *Sci. Rep.*, 2023, **13**(1), 3114.

108 S. Bai, *et al.*, Recent advances of MXenes as electrocatalysts for hydrogen evolution reaction, *npj 2D Mater. Appl.*, 2021, **5**(1), 78.

109 C. Peng, *et al.*, Hybrids of Two-Dimensional Ti3C2 and TiO2 Exposing 001 Facets toward Enhanced Photocatalytic Activity, *ACS Appl. Mater. Interfaces*, 2016, **8**(9), 6051–6060.

110 M. Akbari, *et al.*, MXene-based composite photocatalysts for efficient degradation of antibiotics in wastewater, *Sci. Rep.*, 2024, **14**(1), 31498.

111 P. Kuang, *et al.*, MXene-based photocatalysts, *J. Mater. Sci. Technol.*, 2020, **56**, 18–44.

112 N. H. Solangi, *et al.*, MXene as emerging material for photocatalytic degradation of environmental pollutants, *Coord. Chem. Rev.*, 2023, **477**, 214965.

113 C. Chinnasamy, *et al.*, Recent advancements in MXene-based nanocomposites as photocatalysts for hazardous pollutant degradation - A review, *Environ. Res.*, 2023, **233**, 116459.
114 M. R. Lukatskaya, *et al.*, Cation Intercalation and High Volumetric Capacitance of Two-Dimensional Titanium Carbide, *Science*, 2013, **341**(6153), 1502–1505.
115 G. Fan, *et al.*, Sonophotocatalytic degradation of ciprofloxacin by Bi2MoO6/FeVO4 heterojunction: Insights into performance, mechanism and pathway, *Sep. Purif. Technol.*, 2022, **303**, 122251.
116 S. G. Babu, *et al.*, Synergistic effect of sono-photocatalytic process for the degradation of organic pollutants using CuO-TiO(2)/rGO, *Ultrason. Sonochem.*, 2019, **50**, 218–223.
117 P. Sathishkumar, *et al.*, Sonophotocatalytic (42kHz) degradation of Simazine in the presence of Au–TiO2 nanocatalysts, *Appl. Catal., B*, 2014, **160–161**, 692–700.
118 B. Du, *et al.*, Sonophotocatalytic degradation of 17β-estradiol by Er3+-CdS/MoS2: The role and transformation of reactive oxygen species, *J. Cleaner Prod.*, 2022, **333**, 130203.
119 P. Asaithambi, *et al.*, Distillery industrial wastewater(DIW) treatment by the combination of sono(US), photo(UV) and electrocoagulation(EC) process, *J. Environ. Manage.*, 2022, **320**, 115926.
120 A. Rahmani, *et al.*, The integration of PbO2-based EAOPs with other advanced oxidation processes for improved treatment of water and wastewater, *Curr. Opin. Electrochem.*, 2023, **37**, 101204.
121 G. Eshaq, *et al.*, Superior performance of FeVO4@CeO2 uniform core-shell nanostructures in heterogeneous Fenton-sonophotocatalytic degradation of 4-nitrophenol, *J. Hazard. Mater.*, 2020, **382**, 121059.
122 K. Yun, *et al.*, Fabrication of highly effective Ag6Si2O7/SmFeO3 heterojunction with synergistically enhanced sonophotocatalytic degradation of ciprofloxacin and production of H2O2: Influencing factors and degradation mechanism, *Chem. Eng. J.*, 2023, **468**, 143491.
123 B. Ryu, *et al.*, Degradation synergism between sonolysis and photocatalysis for organic pollutants with different hydrophobicity: A perspective of mechanism and application for high mineralization efficiency, *J. Hazard. Mater.*, 2021, **416**, 125787.
124 D. Meroni, *et al.*, Sonophotocatalytic degradation of sodium diclofenac using low power ultrasound and micro sized TiO2, *Ultrason. Sonochem.*, 2020, **67**, 105123.
125 Y. G. Adewuyi, Sonochemistry: Environmental Science and Engineering Applications, *Ind. Eng. Chem. Res.*, 2001, **40**(22), 4681–4715.
126 T. Li, *et al.*, Fluorine-Free Synthesis of High-Purity Ti3C2T (T=OH, O) via Alkali Treatment, *Angew. Chem., Int. Ed.*, 2018, **57**(21), 6115–6119.
127 Y. B. Li, *et al.*, A general Lewis acidic etching route for preparing MXenes with enhanced electrochemical performance in non-aqueous electrolyte, *Nat. Mater.*, 2020, **19**, 894.
128 S. Vigneshwaran, *et al.*, Enhanced sonophotocatalytic degradation of bisphenol A using bimetal sulfide-intercalated MXenes, 2D/2D nanocomposite, *Sep. Purif. Technol.*, 2020, **250**, 117178.
129 Z. Ding, *et al.*, Ultrasonically synthesized N-TiO2/Ti3C2 composites: Enhancing sonophotocatalytic activity for pollutant degradation and nitrogen fixation, *Sep. Purif. Technol.*, 2021, **276**, 119287.
130 F. Yang, *et al.*, MX@MIL-125(Ti)-mediated sonocatalytic degradation for the dyes and microplastics, *Sep. Purif. Technol.*, 2024, **337**, 126488.
131 K. Saravanakumar, *et al.*, Hierarchical CoTiO3 microrods on Ti3C2Tx MXene heterostructure as an efficient sonocatalyst for bisphenol A degradation, *J. Mol. Liq.*, 2021, **344**, 117740.
132 M. Dai, *et al.*, Rational construction of S-scheme BN/MXene/ZnIn2S4 heterojunction with interface engineering for efficient photocatalytic hydrogen production and chlorophenols degradation, *Sep. Purif. Technol.*, 2023, **309**, 123004.
133 J. L. Torres-García, *et al.*, Bisphenol A in the environment and recent advances in biodegradation by fungi, *Chemosphere*, 2022, **303**, 134940.
134 A. Shahzad, *et al.*, Heterostructural TiO2/Ti3C2Tx (MXene) for photocatalytic degradation of antiepileptic drug carbamazepine, *Chem. Eng. J.*, 2018, **349**, 748–755.
135 Y. Cao, *et al.*, Fabrication of novel CuFe(2)O(4)/MXene hierarchical heterostructures for enhanced photocatalytic degradation of sulfonamides under visible light, *J. Hazard. Mater.*, 2020, **387**, 122021.
136 A. Tariq, *et al.*, Efficient Visible-Light Photocatalysis of 2D-MXene Nanohybrids with Gd(3+)- and Sn(4+)-Codoped Bismuth Ferrite, *ACS Omega*, 2018, **3**(10), 13828–13836.
137 Y. Zhou, *et al.*, Novel dual-effective Z-scheme heterojunction with g-C3N4, Ti3C2 MXene and black phosphorus for improving visible light-induced degradation of ciprofloxacin, *Appl. Catal., B*, 2021, **291**, 120105.
138 X. Zou, *et al.*, Photocatalytic degradation of ranitidine and reduction of nitrosamine dimethylamine formation potential over MXene-Ti(3)C(2)/MoS(2) under visible light irradiation, *J. Hazard. Mater.*, 2021, **413**, 125424.
139 M. A. Iqbal, *et al.*, Ti(3)C(2)-MXene/Bismuth Ferrite Nanohybrids for Efficient Degradation of Organic Dyes and Colorless Pollutants, *ACS Omega*, 2019, **4**(24), 20530–20539.
140 T. Liu, *et al.*, Heterostructured MXene-derived oxides as superior photocatalysts for MB degradation, *J. Alloys Compd.*, 2022, 919.
141 T. Tahir, *et al.*, Synthesis of sponge like Gd3+ doped vanadium oxide/2D MXene composites for improved degradation of industrial effluents and pathogens, *Ceram. Int.*, 2022, **48**(2), 1969–1980.
142 B. Liu, *et al.*, 2D/2D BiOIO3/Ti3C2 MXene nanocomposite with efficient charge separation for degradation of multiple pollutants, *Appl. Surf. Sci.*, 2023, **618**, 156565.

143 H. Zhang, *et al.*, 2D a-Fe2O3 doped Ti3C2 MXene composite with enhanced visible light photocatalytic activity for degradation of Rhodamine B, *Ceram. Int.*, 2018, **44**(16), 19958–19962.
144 L. Yang, *et al.*, Enhanced visible light catalytic activity of holey Ti3C2 based catalyst for azo dyes, *Appl. Surf. Sci.*, 2023, **623**, 157002.
145 L. Cui, *et al.*, Improving the Photocatalytic Activity of Ti(3) C(2) MXene by Surface Modification of N Doped, *Materials*, 2023, **16**(7), 2836.
146 D. Chen, *et al.*, Interfacial Charge Transfer in Defect-Rich Ti3C2/BiOIO3 Heterostructured Photocatalysts for the Degradation of Methyl Orange, *ACS Appl. Nano Mater.*, 2022, **5**(12), 18178–18187.
147 M. Luo, *et al.*, Visible Light Induced g-C3N4/TiO2/Ti3C2 Ternary Z-scheme Heterojunction Photocatalyst for Efficient Degradation, *Electron. Mater. Lett.*, 2022, **19**(1), 94–107.
148 H. Zhang, *et al.*, Designing 3D porous BiOI/Ti3C2 nanocomposite as a superior coating photocatalyst for photodegradation RhB and photoreduction Cr (VI), *Sep. Purif. Technol.*, 2021, **272**, 118911.
149 Z. Wang, *et al.*, Surface -O terminated urchin-like TiO2/Ti3C2O (MXene) as high performance photocatalyst: Interfacial engineering and mechanism insight, *Appl. Surf. Sci.*, 2023, **615**, 156343.
150 Z. Chen, *et al.*, Enhanced photocatalytic degradation of ciprofloxacin by heterostructured BiOCl/Ti3C2Tx MXene nanocomposites, *J. Alloys Compd.*, 2023, **950**, 169797.
151 Y. Bao, *et al.*, Designed 2D/2D/2D Bi2WO6/Ti3C2/SnNb2O6 Z-scheme heterojunction via interfacial chemical bond with enhanced photocatalytic activity, *J. Alloys Compd.*, 2023, **948**, 169762.
152 X. Chen and H. Zhang, Porous ZnS/MXene Ti3C2 nanocomposite with a terrific photocatalytic ability for tetracycline hydrochloride degradation, *Opt. Mater.*, 2023, **141**, 113968.
153 X. Qin, *et al.*, Oxygen vacancy-rich C/Ti3C2/(001)TiO2 hollow microspheres and the photocatalytic degradation of organic pollutants, *Colloids Surf., A*, 2023, **666**, 131258.
154 F.-D. Wu, J.-C. Chen and J.-P. Hu, Synthesis of TiO2/Ti3C2T/AgI Z-scheme photocatalyst for tetracycline hydrochloride photocatalytic degradation, *J. Environ. Chem. Eng.*, 2022, **10**(1), 107117.
155 B. Tan, *et al.*, Construction of Bi2O2CO3/Ti3C2 heterojunctions for enhancing the visible-light photocatalytic activity of tetracycline degradation, *J. Colloid Interface Sci.*, 2021, **601**, 581–593.
156 J. Zhang, *et al.*, Treatment of antibiotics in water by SO3H-modified Ti3C2 Mxene photocatalytic collaboration with g-C3N4, *J. Mater. Sci. Technol.*, 2024, **194**, 124–137.
157 R. Xu, *et al.*, V2C MXene–modified g-C3N4 for enhanced visible-light photocatalytic activity, *J. Alloys Compd.*, 2024, **970**, 172656.
158 J. Li, *et al.*, Solvothermal synthesis of CdTiO3/Ti3C2 MXene composite as a new efficient visible light photocatalyst, *Colloids Surf., A*, 2024, **702**, 134936.
159 W. Tu, *et al.*, Carbon nitride coupled with Ti3C2-Mxene derived amorphous Ti-peroxo heterojunction for photocatalytic degradation of rhodamine B and tetracycline, *Colloids Surf., A*, 2022, **640**, 128448.
160 S. Wang, *et al.*, Effect of HF etching on titanium carbide (Ti3C2Tx) microstructure and its capacitive properties, *Chem. Eng. J.*, 2023, **452**, 139512.
161 M. Ghidiu, *et al.*, Conductive two-dimensional titanium carbide 'clay' with high volumetric capacitance, *Nature*, 2014, **516**(7529), 78–81.
162 D. D. Kruger, H. García and A. Primo, Molten Salt Derived MXenes: Synthesis and Applications, *Advanced Science*, 2024, **11**(35), 2307106.
163 W. Sun, *et al.*, Electrochemical Etching of Ti2AlC to Ti2CTx (MXene) in Low-Concentration Hydrochloric Acid Solution, *J. Mater. Chem. A*, 2017, **5**, 21663.
164 Z. Wei, *et al.*, Alkali treated Ti3C2Tx MXenes and their dye adsorption performance, *Mater. Chem. Phys.*, 2018, **206**, 270–276.
165 U. Khan, *et al.*, Green synthesis of fluorine-free MXene via hydrothermal process: A sustainable approach for proton supercapacitor electrodes, *Electrochim. Acta*, 2024, **475**, 143651.
166 W. Zhang and X. Zhang, The effect of ultrasound on synthesis and energy storage mechanism of Ti3C2Tx MXene, *Ultrason. Sonochem.*, 2022, **89**, 106122.
167 A. Feng, *et al.*, Fabrication and thermal stability of NH4HF2-etched Ti3C2 MXene, *Ceram. Int.*, 2017, **43**(8), 6322–6328.
168 A. Jawaid, *et al.*, Halogen Etch of Ti3AlC2 MAX Phase for MXene Fabrication, *ACS Nano*, 2021, **15**, 2771.